

Power Allocation and Parameter Estimation for Multipath-Based 5G Positioning

Anastasios Kakkavas¹, *Graduate Student Member, IEEE*, Henk Wymeersch², *Senior Member, IEEE*,
Gonzalo Seco-Granados³, *Senior Member, IEEE*, Mario H. Castañeda García⁴, *Member, IEEE*,
Richard A. Stirling-Gallacher⁵, *Member, IEEE*, and Josef A. Nossek⁶, *Life Fellow, IEEE*

Abstract—We consider a single-anchor multiple-input multiple-output orthogonal frequency-division multiplexing system with imperfectly synchronized transmitter (Tx) and receiver (Rx) clocks, where the Rx estimates its position based on the received reference signals. The Tx, having (imperfect) prior knowledge about the Rx location and the surrounding geometry, transmits reference signals based on a set of fixed beams. We develop strategies for the power allocation among the beams aiming to minimize the expected Cramér-Rao lower bound for Rx positioning. Additional constraints on the design are included to make the optimized power allocation robust to uncertainty on the line-of-sight (LOS) path direction. Furthermore, the effect of clock asynchronism on the proposed allocation strategies is studied. Our evaluation results show that, for non-negligible synchronization error, it is optimal to allocate a large fraction of the available power for the illumination of the non-LOS (NLOS) paths, which help resolve the clock offset. In addition, the complexity reduction achieved by our proposed suboptimal approach incurs only a small performance degradation. We also propose an off-grid compressed sensing-based position estimation algorithm, which exploits the information on the clock offset provided by NLOS paths, and show that it is asymptotically efficient.

Index Terms—Positioning, localization, 5G, reference signal, power allocation, parameter estimation.

I. INTRODUCTION

WITH the advent of fifth generation (5G) mobile networks, positioning has attracted lots of research interest. The large chunks of bandwidth available at millimeter-wave (mm-Wave) frequencies as well as the potentially large number of antennas placed at both sides of the communication link are the main driving forces, not only for very high data rates and massive connectivity [1], [2], but also for a drastic improvement of the positioning accuracy of cellular networks [3]. Recently, within the Third Generation Partnership Project (3GPP), new techniques have been standardized, including downlink (DL)-angle of departure (AOD), uplink (UL)-angle of arrival (AOA) and multi-cell round-trip time (RTT) [4], in addition to the already existing ones in previous generations of cellular networks [5], such as observed time difference of arrival (OTDOA) and uplink TDOA (UTDOA). Furthermore, proposals for reporting delay and angular multipath measurements to enable single-anchor positioning have been considered [6]. With their enhanced positioning capabilities, 5G systems aim to accommodate use cases like autonomous driving [7], augmented reality and industrial internet of things (IIoT) [6].

Single-anchor localization has received increasing attention in recent years. Leveraging the high temporal and angular resolution of mm-Wave multiple-input multiple-output (MIMO) systems, it has the potential to ease the requirements of multi-anchor hearability and interference management. The fundamental limits of single-anchor positioning were investigated in [8]–[12].

Single-anchor localization algorithms in the literature can be classified into two categories: one-shot schemes without tracking [13]–[20], and approaches with tracking [21]–[27]. While the latter mainly focus on position estimation and tracking given the channel parameter measurements, the former also deal with the estimation of the channel parameters, as done in this work. A three-stage algorithm for the estimation of the user equipment (UE) state (position and orientation) with a MIMO-orthogonal frequency-division multiplexing (OFDM) system was proposed in [13], where in the first stage a compressed sensing-based algorithm is used to obtain coarse estimates of the multipath parameters (number of paths,

Manuscript received August 6, 2020; revised February 1, 2021 and May 4, 2021; accepted May 6, 2021. Date of publication May 28, 2021; date of current version November 11, 2021. This work was supported in part by the EU-H2020 project Fifth Generation Communication Automotive Research and Innovation (5GCAR) and in part by the Catalan Institution for Research and Advanced Studies (ICREA) Academia Program and the Spanish Ministry of Science, Innovation and Universities Project under Grant TEC2017-89925-R. The associate editor coordinating the review of this article and approving it for publication was M. Ding. (*Corresponding author: Anastasios Kakkavas.*)

Anastasios Kakkavas is with the Munich Research Center, Huawei Technologies Duesseldorf GmbH, 80992 Munich, Germany, and also with the Department of Electrical and Computer Engineering, Technical University of Munich, 80333 Munich, Germany (e-mail: anastasios.kakkavas@huawei.com).

Henk Wymeersch is with the Department of Electrical Engineering, Chalmers University of Technology, 412 58 Gothenburg, Sweden (e-mail: henkw@chalmers.se).

Gonzalo Seco-Granados is with the Department of Telecommunications and Systems Engineering, Universitat Autònoma de Barcelona (UAB), 08193 Bellaterra, Spain (e-mail: gonzalo.seco@uab.cat).

Mario H. Castañeda García and Richard A. Stirling-Gallacher are with the Munich Research Center, Huawei Technologies Duesseldorf GmbH, 80992 Munich, Germany (e-mail: mario.castaneda@huawei.com; richard.sg@huawei.com).

Josef A. Nossek is with the Department of Electrical and Computer Engineering, Technical University of Munich, 80333 Munich, Germany (e-mail: josef.a.nossek@tum.de).

Color versions of one or more figures in this article are available at <https://doi.org/10.1109/TWC.2021.3082581>.

Digital Object Identifier 10.1109/TWC.2021.3082581

time of arrivals (TOAs), AODs, AOA and gains), with the coarse estimates refined in the second stage. In the third stage, the refined estimates are mapped to the receiver (Rx) position and orientation and the scatterer/reflector positions using the extended invariance principle (EXIP). A similar approach is followed in [14], with the main difference being the mapping from channel parameters to position parameters, where an iterative Gibbs sampling method is employed. In [15] range-free angle-based approaches are developed assuming prior map information. An algorithm for localization and synchronization of cooperating full-duplex agents using a single-anchor is developed in [16]. Furthermore, the authors of [17] propose a protocol and an accompanying algorithm that enables a single-anchor to (quasi-)simultaneously receive messages from multiple agents in order to localize them using TOA and AOA measurements. A DL positioning algorithm for a single-antenna Rx, based on TOA and AOD measurements is proposed in [19]. The work is extended in [20], where a two-step process is used, with the coarse parameter estimates obtained in the first step used for adaptation of the transmitter (Tx) beamforming matrix in the second step. Additionally, in [28] an iterative Tx beamforming refinement and position estimation algorithm is developed.

Similar to [20], [28], many works have considered the use of prior knowledge of the Rx position at the Tx to design beamformers that improve the Rx's localization accuracy. In [29] Cramér-Rao lower bound (CRLB)-optimal precoders for tracking the AOD and AOA of a path were designed, taking the uncertainty about their value into account. In [30], assuming a line-of-sight (LOS) channel and a multicarrier system, beamformers minimizing the TOA and AOA error bounds were proposed, based on the current estimate of the Rx position. Using a similar setup, but additionally considering multiple users, the authors of [31] designed beamformers maximizing a weighted sum of Fisher information on delay, AOD and AOA. Although in a different context, the algorithms and conclusions of [32] and [33] are relevant to our Tx beamforming problem. In [32] and [33], robust beamformers under angular uncertainty were designed and it was concluded that the Rx steering vector and its derivative contain all the localization information. Again in a different but still relevant setup, the authors of [34] and [35] computed the optimal power allocation among multiple anchors for ranging-based localization by solving a semidefinite program (SDP). The power allocation problem is formulated as the computation of either the optimal sharing of a fixed available total power budget among the network anchors so as to minimize the squared position error bound (SPEB) of a target or the power allocation vector with the minimum sum power that satisfies a set of predefined positioning accuracy constraints. Similar approaches were considered in [36] and [37]. In [38] it was further shown that, when the uncertainty about the Rx position is not considered, it is optimal to transmit only on the directions corresponding to the Tx array steering vector and its derivative. The power allocation among these two directions minimizing the SPEB was then analytically calculated in [38]. When the Rx location uncertainty is taken into account, the optimal power allocation among the beams of a given

Tx beam codebook was computed to minimize the average or maximum SPEB.

In this paper, we extend our work in [38]. We consider a single-anchor setup and a sparse multipath channel, which comprises the LOS path and a number of single-bounce non-LOS (NLOS) paths, as multi-bounce paths are considered too weak for reception at mm-Wave frequencies [39]–[42]. The Tx has only a coarse prior knowledge of the underlying geometry and in addition, the Tx-Rx clocks are imperfectly synchronized. We optimize the power allocation on a beam codebook for the multipath channel and examine the effect of imperfect synchronization on the resulting power allocation. The power allocation is based on the CRLB, which provides a fundamental lower bound on the covariance of the estimation error of any (unbiased) estimator. Hence, the power allocation can be performed without knowledge of the position estimation algorithm and only the statistics of the UE state and environment are needed. This is a benefit compared to an algorithm-dependent allocation. We also develop a novel position estimation algorithm, which is evaluated for the proposed power allocation strategies. The main contributions of the work can be summarized as follows:

- We propose power allocation strategies on a fixed Tx beam codebook with the aim of minimizing the expected positioning error of the Rx. The optimal solution and a suboptimal one with lower computational complexity are presented and evaluated.
- We develop a two-stage position estimation algorithm. The first stage consists of an off-grid channel parameter estimation algorithm, based on [43]. The second stage maps the channel parameter estimates to position parameters. The information about the clock offset offered by NLOS paths in combination with the LOS path is exploited so as to discard false alarms.

We note that although a two-dimensional (2D) scenario is considered in the paper, the fundamental conclusions also hold in a three-dimensional (3D) setup: the global optimum power allocation can be decoupled in intra-path power allocation and inter-path power allocation, and the first one can be done path by path. Also, the quality of Tx-Rx synchronization impacts the amount of power allocated for NLOS paths illumination, so as to help the Rx resolve the clock offset. The power allocation strategies can be easily adapted to a 3D setup. As far as the position estimation algorithm is concerned, both the channel parameter estimation and the mapping to position can be extended to a 3D setup. Nevertheless, the increased complexity of the grid search step used in the proposed channel parameter estimation could potentially require further consideration.

The rest of the paper is organized as follows. In Sec. II we present the system model and the assumptions of the work. The theoretical bound on positioning accuracy is briefly discussed in Sec. III and the proposed power allocation methods are presented in Sec. IV. The position estimation algorithm is introduced in Sec. V and numerical evaluations of the proposed approaches are provided in Sec. VI. Finally, Sec. VII concludes the work.

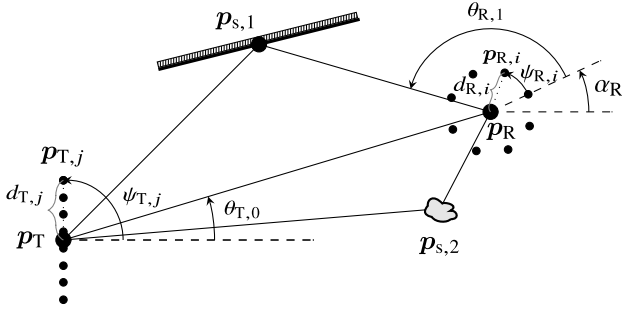


Fig. 1. Geometric model, example with a uniform linear array (ULA) at the Tx and a uniform circular array (UCA) at the Rx.

Notation: We use bold lowercase for vectors, bold uppercase for matrices, non-bold for scalars and calligraphic letters for sets. Depending on its argument, $|\cdot|$ denotes the absolute value of a scalar, the determinant of a matrix or the cardinality of a set. The transpose, conjugate transpose and p -norm of a vector/matrix are denoted by $(\cdot)^T$, $(\cdot)^H$ and $\|\cdot\|_p$ and the Frobenius norm of a matrix is denoted by $\|\cdot\|_F$. $\Re\{\cdot\}$ and $\Im\{\cdot\}$ denote the real and imaginary part of a complex number and $\arg(\cdot)$ denotes its phase. The i -th element of a vector and the (i, j) -th element of a matrix are denoted by $[\cdot]_i$ and $[\cdot]_{i,j}$, respectively. \mathbf{I}_n , $\mathbf{1}$ and $\mathbf{0}$ denote the identity matrix of size n , and the all-ones and all-zeros matrix of the appropriate size. $\text{diag}(\mathbf{x})$ denotes the diagonal matrix with the elements of \mathbf{x} on its diagonal. The expectation operator is denoted by $\mathbb{E}[\cdot]$ and the sets of real and complex numbers are denoted by \mathbb{R} and \mathbb{C} . A multivariate (circularly symmetric complex) Gaussian distribution with mean $\boldsymbol{\mu}$ and covariance matrix \mathbf{C} is denoted by $\mathcal{N}(\boldsymbol{\mu}, \mathbf{C})$ ($\mathcal{N}_{\mathbb{C}}(\boldsymbol{\mu}, \mathbf{C})$). The Hessian of a function $f(\mathbf{x})$ is denoted as $D_{\mathbf{x}}^2 f(\mathbf{x})$.

II. SYSTEM MODEL AND ASSUMPTIONS

A. Geometric Model

The Tx consists of an array with N_T antennas and reference point located at the origin. The Rx consists of an array with N_R antennas, a reference point located at $\mathbf{p}_R = [p_{R,x}, p_{R,y}]^T \in \mathbb{R}^2$ and orientation α_R . The position of the j -th element of the Tx array is given by

$$\mathbf{p}_{T,j} = d_{T,j} \mathbf{u}(\psi_{T,j}) \in \mathbb{R}^2, \quad j = 0, \dots, N_T - 1, \quad (1)$$

where $\mathbf{u}(\psi) = [\cos(\psi), \sin(\psi)]^T$ and $d_{T,j}$ and $\psi_{T,j}$ are its distance and angle from the Tx array's reference point, as shown in Fig. 1. The position of the i -th element of the Rx array is

$$\mathbf{p}_{R,i} = \mathbf{p}_R + d_{R,i} \mathbf{u}(\psi_{R,i} + \alpha_R) \in \mathbb{R}^2, \quad i = 0, \dots, N_R - 1. \quad (2)$$

We assume that for all antenna pairs there are L discrete propagation paths. The first of these L paths ($l = 0$) is the LOS path and the rest ($l = 1, \dots, L - 1$) are single-bounce NLOS paths. The point of incidence of the l -th single-bounce path, which corresponds either to scattering or reflection, is $\mathbf{p}_{s,l} = [p_{s,l,x}, p_{s,l,y}]^T$, $l = 1, \dots, L - 1$. The array apertures are assumed to be small compared to the distance between Tx and Rx, as well as the distance between each of the scatterers/reflectors and the Tx or Rx. Therefore, the delay

of the l -th path from Tx element j to Rx element i can be approximated by [12]

$$\tau_{l,i,j} \approx \tau'_l - \tau_{T,j}(\theta_{T,l}) - \tau_{R,i}(\theta_{R,l}), \quad l = 0, \dots, L - 1, \quad (3)$$

where

$$\tau'_l = \begin{cases} \|\mathbf{p}_R\|_2/c, & l = 0, \\ (\|\mathbf{p}_{s,l}\|_2 + \|\mathbf{p}_R - \mathbf{p}_{s,l}\|_2)/c, & l \neq 0, \end{cases} \quad (4)$$

$$\tau_{T,j}(\theta_{T,l}) = d_{T,j} \mathbf{u}^T(\psi_{T,j}) \mathbf{u}(\theta_{T,l})/c, \quad (5)$$

$$\tau_{R,i}(\theta_{R,l}) = d_{R,i} \mathbf{u}^T(\psi_{R,i}) \mathbf{u}(\theta_{R,l})/c, \quad (6)$$

with c being the speed of light. The angles are defined as

$$\theta_{T,l} = \begin{cases} \text{atan2}(p_{R,y}, p_{R,x}), & l = 0, \\ \text{atan2}(p_{s,l,y}, p_{s,l,x}), & l \neq 0, \end{cases} \quad (7)$$

$$\theta_{R,l} = \begin{cases} \theta_{T,l} + \pi - \alpha_R, & l = 0, \\ \text{atan2}(p_{s,l,y} - p_{R,y}, p_{s,l,x} - p_{R,x}) - \alpha_R, & l \neq 0, \end{cases} \quad (8)$$

with $\text{atan2}(y, x)$ being the four-quadrant inverse tangent function.

B. Signal Model

An OFDM waveform with subcarrier spacing Δf , N subcarriers and cyclic prefix (CP) duration T_{CP} is considered. The reference signal is transmitted on N_p subcarriers, whose indices are described by $\mathcal{P} = \{p_1, \dots, p_{N_p}\}$ and N_B OFDM symbols are transmitted. We assume a narrowband signal model, i.e., $B/f_c \ll \lambda_c/D_{\max}$, where $B \approx \Delta f(\max(\mathcal{P}) - \min(\mathcal{P}))$ is the signal bandwidth, f_c is the carrier frequency, λ_c is the carrier wavelength and D_{\max} is the largest of the Tx and Rx array apertures. The reference signal resource grid \mathcal{R} comprises all resource elements at the time-frequency points (p, b) , $p \in \mathcal{P}$, $b = 0, \dots, N_B - 1$. The transmitter uses a beam codebook $\{\mathbf{f}_k\}_{k=1}^{M_T}$, where M_T is the number of beams in the codebook and $\|\mathbf{f}_k\|_2 = 1, \forall k$. The k -th beam is used on a subset \mathcal{R}_k of resource elements (REs) (p, b) , with $\mathcal{R}_k \cap \mathcal{R}_{k'} = \emptyset$ for $k \neq k'$. The transmitted signal vector at the p -th subcarrier, $p \in \mathcal{P}$, of the b -th OFDM symbol, $b = 0, \dots, N_B - 1$, then is

$$\mathbf{x}[p, b] = \lambda_k[p, b] \mathbf{f}_k, \quad (p, b) \in \mathcal{R}_k, \quad (9)$$

where

$$\lambda_k[p, b] = \sqrt{P_{\text{tot}} q_k \gamma_k[p, b]} e^{j\beta_k[p, b]} \quad (10)$$

is the symbol assigned to \mathbf{f}_k at the p -th subcarrier, P_{tot} is the total Tx power (disregarding the power used for the CP), q_k is the fraction of P_{tot} allocated to \mathbf{f}_k , with $\sum_{k=1}^{M_T} q_k = 1$, $\gamma_k[p, b]$ is the fraction of q_k allocated to the RE (p, b) , with $\sum_{(p,b) \in \mathcal{R}_k} \gamma_k[p, b] = 1$, and $\beta_k[p, b]$ is the phase of $\lambda_k[p, b]$. The received signal is

$$\mathbf{y}[p, b] = \mathbf{m}[p, b] + \boldsymbol{\eta}[p, b], \quad (11)$$

where

$$\mathbf{m}[p, b] = \sum_{l=0}^{L-1} h_l e^{-j\omega_p \tau_l} \mathbf{a}_R(\theta_{R,l}) \mathbf{a}_T^T(\theta_{T,l}) \mathbf{x}[p, b], \quad (12)$$

$$\mathbf{a}_T(\theta_{T,l}) = [e^{j\omega_c \tau_{T,1}(\theta_{T,l})}, \dots, e^{j\omega_c \tau_{T,N_T}(\theta_{T,l})}]^T \in \mathbb{C}^{N_T} \quad (13)$$

is the Tx array steering vector, with the Rx steering vector $\mathbf{a}_R(\theta_{R,l})$ defined accordingly, and

$$\tau_l = \tau'_l + \epsilon_{\text{clk}}, \quad (14)$$

with ϵ_{clk} being the clock offset, which describes the mismatch between the clocks at the Tx and Rx devices. Also, $\omega_p = 2\pi p \Delta f$, $\omega_c = 2\pi f_c$, h_l is the gain of the l -th path and $\boldsymbol{\eta}[p, b] \sim \mathcal{N}_{\mathbb{C}}(\mathbf{0}, \sigma_{\eta}^2 \mathbf{I}_{N_R})$ is the additive white Gaussian noise (AWGN). The gains h_l are assumed to be time-invariant, therefore the channel is assumed to be quasi-static for N_B OFDM symbols.

The clock offset, which arises from imperfect Tx-Rx clock synchronization, appears in the signal model (11)-(14) in the following way. In general, the received signal depends on the absolute TOAs, which are equal to the sum of the respective path delays τ'_l and the time of departure (TOD). To extract information on the path delays, which can then be translated to position information via (4), the TOD has to be known and its effect on the received signal removed. The effect of the TOD on the received signal can be perfectly removed if the Rx knows the TOD and if the Tx and Rx clocks are perfectly synchronized. However, in practical systems, where an actual time synchronization method is employed, e.g. [44], [45], an offset ϵ_{clk} between the clocks is present and effectively added to the observed path delays τ_l (14). The clock offset ϵ_{clk} is assumed to be a zero-mean Gaussian random variable with variance σ_{clk}^2 [10], [46], [47]. When $\sigma_{\text{clk}} \rightarrow 0$, the clocks are perfectly synchronized, while $\sigma_{\text{clk}} \rightarrow \infty$ corresponds to asynchronous operation. In the latter case, each TOA cannot be reliably mapped to a path delay and only differences between TOAs (if more than one paths are available) can provide position information.

We write the signal model (11) as

$$\mathbf{Y}_b = \sum_{l=0}^{L-1} h_l \mathbf{C}_b(\tau_l, \theta_{T,l}, \theta_{R,l}) + \mathbf{N}_b, \quad (15)$$

where

$$\mathbf{C}_b(\tau_l, \theta_{T,l}, \theta_{R,l}) = \mathbf{a}_R(\theta_{R,l}) \mathbf{a}_T^T(\theta_{T,l}) \mathbf{X}_b \times \text{diag}(\mathbf{a}_{\tau}(\tau_l)) \in \mathbb{C}^{N_R \times N_P}, \quad (16)$$

$$\mathbf{a}_{\tau}(\tau) = [e^{-j\omega_{p_1} \tau}, \dots, e^{-j\omega_{p_{N_P}} \tau}]^T \in \mathbb{C}^{N_P}, \quad (17)$$

$$\mathbf{Y}_b = [\mathbf{y}[p_1, b], \dots, \mathbf{y}[p_{N_P}, b]] \in \mathbb{C}^{N_R \times N_P}, \quad (18)$$

$$\mathbf{X}_b = [\mathbf{x}[p_1, b], \dots, \mathbf{x}[p_{N_P}, b]] \in \mathbb{C}^{N_T \times N_P}, \quad (19)$$

$$\mathbf{N}_b = [\boldsymbol{\eta}[p_1, b], \dots, \boldsymbol{\eta}[p_{N_P}, b]] \in \mathbb{C}^{N_R \times N_P}. \quad (20)$$

Stacking the observations over N_B OFDM symbols we get

$$\mathbf{Y} = \sum_{l=0}^{L-1} h_l \mathbf{C}(\tau_l, \theta_{T,l}, \theta_{R,l}) + \mathbf{N}, \quad (21)$$

where

$$\mathbf{Y} = [\mathbf{Y}_0^T, \dots, \mathbf{Y}_{N_B-1}^T]^T, \quad (22)$$

$$\mathbf{C}(\tau, \theta_T, \theta_R) = [\mathbf{C}_0^T(\tau, \theta_T, \theta_R), \dots, \mathbf{C}_{N_B-1}^T(\tau, \theta_T, \theta_R)]^T, \quad (23)$$

$$\mathbf{N} = [\mathbf{N}_0^T, \dots, \mathbf{N}_{N_B-1}^T]^T. \quad (24)$$

Through (4), (7)-(8) and (21), we can see that the observations \mathbf{Y} depend on the position parameter vector $\boldsymbol{\nu}$, defined as

$$\boldsymbol{\nu} = [\mathbf{p}_R^T, \alpha_R, \epsilon_{\text{clk}}, \mathbf{h}_0^T, \mathbf{p}_{s,1}^T, \mathbf{h}_1^T, \dots, \mathbf{p}_{s,L-1}^T, \mathbf{h}_{L-1}^T]^T \in \mathbb{R}^{4L+2}, \quad (25)$$

with $\mathbf{h}_l = [|h_l|, \arg(h_l)]^T$.

C. Assumptions

1) *Reference Signal Structure*: In this work we consider the case where Tx uses a fixed beam codebook \mathbf{f}_k , $k = 1, \dots, M_T$. This does not only simplify the optimization task, but also might be a practical limitation in a 5G system, with devices using a predefined set of beams for transmission or reception.

We also assume that the resource allocation \mathcal{R}_k among the codebook beams and the power allocation $\gamma_k[p, b]$ among assigned REs, are fixed and therefore, optimizing \mathcal{R}_k is not in the scope of our reference signal optimization task. The problem of designing a waveform has been addressed in [48]–[50], where the CRLB and the Ziv-Zakai lower bound (ZZLB) for range estimation [48], the joint CRLB of time-delay and channel estimation [49], as well as the CRLB of the UE position under robustness constraints [50], have been optimized with respect to the resource allocation.

2) *Prior Knowledge at Rx and Tx*: In many cases the Tx might have prior knowledge on $\boldsymbol{\nu}$, based on prior estimation in the reverse link, map information and known geographical distribution of the users. For example, the base station (BS) can make use of preceding UL sounding reference signal (SRS) transmissions to estimate the UE position and the position of the scatterers. The estimation algorithm can also exploit map information, if available, e.g. location of walls and other objects in an indoor setup. The estimation algorithm could either provide estimates of the distributions directly [26] or provide point estimates [13], for which the BS can then assume a distribution (e.g. Gaussian with variance equal to the corresponding CRLB, evaluated at the point estimates). Alternatively, the UE may have an estimate of its position, as well as a quality measure of this estimate, either from an external source (e.g. Global Navigation Satellite System (GNSS)) or from a previous DL transmission (e.g. DL positioning reference signal (PRS)) and shares them with the BS. The prior information is encoded by the joint probability density function (pdf) $p_{\boldsymbol{\nu}}(\boldsymbol{\nu})$. In the following, we examine how the Tx can exploit the prior information, so as to improve the ability to localize the Rx.

The Rx, which aims to compute its position and orientation from the received signal, only has knowledge on the clock offset's distribution $p_{\epsilon_{\text{clk}}}$.

III. POSITION ERROR BOUND

The achievable positioning accuracy of the Rx can be characterized in terms of the hybrid CRLB. For a parameter vector $\boldsymbol{\nu}$ containing both deterministic and random parameters,

the covariance matrix \mathbf{C} of any unbiased estimator $\hat{\nu}$ of ν satisfies [51], [52]

$$\mathbf{C} - \mathbf{J}_\nu^{-1} \succeq \mathbf{0}, \quad (26)$$

where $\succeq \mathbf{0}$ denotes positive semi-definiteness and $\mathbf{J}_\nu \in \mathbb{R}^{(4L+2) \times (4L+2)}$ is the hybrid Fisher information matrix (FIM) of ν . \mathbf{J}_ν is defined as

$$\mathbf{J}_\nu = \mathbf{J}_\nu^{(p)} + \mathbf{J}_\nu^{(o)}, \quad (27)$$

where

$$\mathbf{J}_\nu^{(p)} = \mathbb{E}_{\nu_r}[-D_\nu^2 \ln p(\nu_r)] \quad (28)$$

accounts for the prior information and

$$\mathbf{J}_\nu^{(o)} = \mathbb{E}_{\mathbf{Y}, \nu_r}[-D_\nu^2 \ln p(\mathbf{Y}|\nu)] \quad (29)$$

accounts for the observation-related information, with ν_r representing the random parameters in ν . As ϵ_{clk} is the only parameter with prior information at the Rx, it is straightforward to find that, based on (25), the only non-zero entry of $\mathbf{J}_\nu^{(p)}$ is

$$[\mathbf{J}_\nu^{(p)}]_{4,4} = 1/\sigma_{\text{clk}}^2. \quad (30)$$

Since ν is observed under AWGN, the (i, j) -th entry of the $\mathbf{J}_\nu^{(o)}$ is

$$[\mathbf{J}_\nu^{(o)}]_{i,j} = \frac{2}{\sigma_\eta^2} \sum_{b=1}^{N_B} \sum_{p \in \mathcal{P}} \Re \left\{ \frac{\partial \mathbf{m}_b^H[p]}{\partial \nu_i} \frac{\partial \mathbf{m}_b[p]}{\partial \nu_j} \right\}. \quad (31)$$

Using (4), (12) and (31), we can see that $\mathbf{J}_\nu^{(o)}$ is independent of the value of ϵ_{clk} . The SPEB is defined as

$$\text{SPEB} = \text{tr}(\mathbf{E}^T \mathbf{J}_\nu^{-1} \mathbf{E}), \quad (32)$$

where $\mathbf{E} = [e_1, e_2]$ and e_i is the i -th column of the identity matrix of the appropriate size. The position error bound (PEB) is defined as its square root.

IV. BEAM POWER ALLOCATION OPTIMIZATION

For the reference signal optimization, we make use of the assumption that with large bandwidth and number of antennas the paths are asymptotically orthogonal [9], [12]. We note that the SPEB is a function of

$$\begin{aligned} \nu' &= [\mathbf{p}_R^T, \alpha_R, |h_0|, \mathbf{p}_{s,1}^T, |h_1|, \dots, \mathbf{p}_{s,L-1}^T, |h_{L-1}|]^T \\ &\in \mathbb{R}^{3L+1}, \end{aligned} \quad (33)$$

that is, it is independent of the values of $\arg(h_l)$, $l = 1, \dots, L-1$, and ϵ_{clk} . Also, due to the inner product of the derivatives in (31), we can observe (see (9), (10) and (12)) that \mathbf{J} is independent of $\beta_k[p, b]$. In the following, we write $\mathbf{J}_\nu = \mathbf{J}_\nu(\mathbf{q}, \nu')$, with $\mathbf{q} = [q_1, \dots, q_{M_T}] \in \mathbb{R}^{M_T}$, to stress that \mathbf{J}_ν is the hybrid FIM of ν , whose value depends on \mathbf{q} and ν' . Similarly, we write $\text{SPEB} = \text{SPEB}(\mathbf{q}, \nu')$.

We study how the Tx can optimize the beam power allocation \mathbf{q} using its prior knowledge on ν' so as to enable higher positioning accuracy at the Rx. We choose the expected SPEB (ESPEB)

$$\text{ESPEB} = \mathbb{E}_{\nu'}[\text{SPEB}(\mathbf{q}, \nu')] \quad (34)$$

as the performance metric. The optimization problem in hand reads as:

$$\min_{\mathbf{q}} \mathbb{E}_{\nu'}[\text{SPEB}(\mathbf{q}, \nu')] \quad \text{s.t.} \quad \mathbf{q} \succcurlyeq \mathbf{0}, \mathbf{1}^T \mathbf{q} \leq 1, \quad (35)$$

where \succcurlyeq denotes element-wise inequality.

A. Optimal Solution

In order to solve (35), one can employ a cubature rule [53], [54] with positive weights to approximate the expectation integral with a sum:

$$\mathbb{E}_{\nu'}[\text{SPEB}(\mathbf{q}, \nu')] \approx \sum_{j=1}^{N_{\nu'}} p_j \text{SPEB}(\mathbf{q}, \nu'_j), \quad (36)$$

where ν'_j and $p_j > 0$, $j = 1, \dots, N_{\nu'}$ are the cubature points and their corresponding weights, with $N_{\nu'}$ being the number of cubature points. $N_{\nu'}$ is determined by the dimension of ν' and the degree r of the cubature.¹ The cubature points and their weights are determined by the pdf of ν' and r . Then, (35) becomes

$$\min_{\mathbf{q}} \sum_{j=1}^{N_{\nu'}} p_j \text{SPEB}(\mathbf{q}, \nu'_j) \quad \text{s.t.} \quad \mathbf{q} \succcurlyeq \mathbf{0}, \mathbf{1}^T \mathbf{q} \leq 1. \quad (37)$$

In a similar fashion to [38], using the epigraph form of (37), we can show that it is equivalent to the following SDP:

$$\begin{aligned} \min_{\mathbf{q}, \mathbf{B}_1, \dots, \mathbf{B}_{N_{\nu'}}} \quad & \sum_{j=1}^{N_{\nu'}} p_j \text{tr}(\mathbf{B}_j) \\ \text{s.t.} \quad & \begin{bmatrix} \mathbf{B}_j & \mathbf{E}^T \\ \mathbf{E} & \mathbf{J}(\mathbf{q}, \nu'_j) \end{bmatrix} \succeq \mathbf{0}, \quad j = 1, \dots, N_{\nu'}, \\ & \mathbf{q} \succcurlyeq \mathbf{0}, \mathbf{1}^T \mathbf{q} \leq 1, \end{aligned} \quad (38)$$

where $\mathbf{B}_j \in \mathbb{R}^{2 \times 2}$, $j = 1, \dots, N_{\nu'}$, are auxiliary variables of the SDP and \succeq denotes positive semidefiniteness. The positivity requirement on the cubature weights is imposed to ensure convexity of the objective in (38).

The optimal vector \mathbf{q} obtained with (38) may indicate that a very small fraction of the available power should be allocated in the direction of the LOS path, which may lead to a missed detection of the LOS path at the Rx. This can be avoided by ensuring that the excitation on directions around the LOS path is at least a fraction q_{th} of the excitation in any other direction. To this end, for a given confidence level κ , we define $\theta_{T,l,\min}^{(\kappa)}$ and $\theta_{T,l,\max}^{(\kappa)}$ as the minimum and maximum AODs corresponding to the 2D Rx locations ($l = 0$) or scatterer/reflector locations ($l = 1, \dots, L-1$) in the κ -confidence ellipse of the respective marginal. With a uniform grid of N_θ possible AODs $\theta_{T,l,m}$ within the interval $[\theta_{T,l,\min}^{(\kappa)}, \theta_{T,l,\max}^{(\kappa)}]$

$$\theta_{T,l,m}^{(\kappa)} = \theta_{T,l,\min}^{(\kappa)} + \frac{m-1}{N_\theta-1} \theta_{T,l,\max}^{(\kappa)}, \quad m = 1, \dots, N_\theta, \quad (39)$$

we define the excitation matrix $\mathbf{A}_l \in \mathbb{R}^{N_\theta \times M_T}$ for the l -th path as

$$[\mathbf{A}_l]_{m,k} = |\mathbf{a}_T^T(\theta_{T,l,m}^{(\kappa)}) \mathbf{f}_k|^2. \quad (40)$$

¹A cubature rule has degree r if it is exact for a (multivariate) polynomial of degree r .

Finally, the excitation vector for the possible AODs of the l -th path is $\mathbf{A}_l \mathbf{q}$. We augment (38) with the following linear constraints:

$$\mathbf{A}_0 \mathbf{q} \succeq q_{\text{th}} \|\mathbf{A} \mathbf{q}\|_{\infty} \mathbf{1}_{N_{\theta}}, \quad (41)$$

where $\mathbf{A} = [\mathbf{A}_0^T, \dots, \mathbf{A}_{L-1}^T]^T$. We note that the constraints (41) are equivalent to

$$\mathbf{A}_0 \mathbf{q} \succeq q_{\text{th}} e_{\text{max}} \mathbf{1}_{N_{\theta}}, \quad \mathbf{A} \mathbf{q} \preceq e_{\text{max}} \mathbf{1}_{LN_{\theta}}, \quad (42)$$

with e_{max} being an auxiliary optimization variable. We refer to the optimal vector \mathbf{q} obtained with (38) as the optimized unconstrained solution (opt. unconstr.). The optimal vector \mathbf{q} obtained with (38) under the constraints (41) is referred as the optimized constrained solution (opt. constr.).

The main challenge with the solutions described above is that p_{ν} is a multidimensional pdf. The number of auxiliary matrices \mathbf{B}_j and corresponding positive semidefiniteness (PSD) constraints in (38) is equal to the number of cubature points. For known cubature rules [53], the number of points is lower bounded by $(3L+1)^{(r-1)/2}$, which could result in very high complexity for our optimization task, as the integrand is highly non-linear and a rule with $r \geq 5$ is required for an accurate approximation.

B. Dimensionality Reduction

A way to circumvent the dimensionality challenge is to use a surrogate function which involves the expectation over a smaller set of parameters. To this end, we first note that $e_i^T \mathbf{J}^{-1} \mathbf{e}_i$, $i = 1, 2$, is a convex function of \mathbf{J} and so is the SPEB as a sum of convex functions. Splitting ν' into any couple of vectors ν_1 and ν_2 , we can write

$$\begin{aligned} & \mathbb{E}_{\nu}[\text{SPEB}(\mathbf{q}, \nu)] \\ &= \mathbb{E}_{\nu}[\text{tr}(\mathbf{E}^T \mathbf{J}^{-1}(\mathbf{q}, \nu') \mathbf{E})] \\ &= \mathbb{E}_{\nu_1}[\mathbb{E}_{\nu_2|\nu_1}[\text{tr}(\mathbf{E}^T \mathbf{J}^{-1}(\mathbf{q}, \nu_1, \nu_2) \mathbf{E})]] \\ &\stackrel{(a)}{\geq} \mathbb{E}_{\nu_1}[\text{tr}(\mathbf{E}^T (\mathbb{E}_{\nu_2|\nu_1}[\mathbf{J}(\mathbf{q}, \nu_1, \nu_2)])^{-1} \mathbf{E})] \end{aligned} \quad (43)$$

where (a) follows from Jensen's inequality. We choose $\nu_1 = [\mathbf{p}_R^T, \mathbf{p}_{s,1}^T, \dots, \mathbf{p}_{s,L-1}^T]^T$ and $\nu_2 = [\alpha_R, |h_0|, |h_1|, \dots, |h_{L-1}|]^T$, as the position parameters are the ones determining the AODs, which in turn determine which beams are relevant or not. One could optimize the lower bound on the ESPEB (ESPEB) given in (43), as described in (35)-(38). We refer to the resulting solution as the optimal solution with reduced dimensionality (opt. reduced). The number of required cubature points $N_{\nu'}$ is still lower bounded by $(2L)^{(r-1)/2}$.

C. Low-Complexity Suboptimal Solution

Our aim is to reduce the complexity of the optimization problem in hand. We accomplish this by taking the following heuristic approach: we compute a power allocation vector \mathbf{q}_l , $l = 0, \dots, L-1$, considering the uncertainty regarding each path separately. We then weight the resulting power allocation vectors in order to minimize a lower bound on the ESPEB, with the final power allocation vector being the weighted sum of the per-path power allocation vectors.

More specifically, for the power allocation vector \mathbf{q}_0 , we consider only the LOS path and neglect the NLOS paths and solve

$$\begin{aligned} \mathbf{q}_0 &= \text{argmin}_{\mathbf{q}} \mathbb{E}_{\mathbf{p}_R} [\text{tr}(\mathbf{E}^T (\mathbb{E}_{|h_0|, \alpha_R | \mathbf{p}_R} [\mathbf{J}_{\nu_{\text{LOS}}}(\mathbf{q}, \mathbf{p}_R, \alpha_R, |h_0|)])^{-1} \mathbf{E})] \\ \text{s.t. } \mathbf{A}_0 \mathbf{q} &\succeq q_{\text{th, LOS}} \|\mathbf{A}_0 \mathbf{q}\|_{\infty} \mathbf{1}_{N_{\theta}}, \quad \mathbf{q} \succeq \mathbf{0}, \quad \mathbf{1}^T \mathbf{q} \leq 1, \end{aligned} \quad (44)$$

where $\mathbf{J}_{\nu_{\text{LOS}}}$ represents the FIM for the parameter vector $\nu_{\text{LOS}} = [\mathbf{p}_R^T, \alpha_R, \epsilon_{\text{clk}}, \mathbf{h}_0^T]^T$. Similarly to (41), the first constraint in (44) limits the ratio of power used among possible LOS directions, with $q_{\text{th, LOS}}$ being the corresponding minimum ratio. For the gain of the LOS path it is natural that $p(\mathbf{h}_0 | \mathbf{p}_R) = p(\mathbf{h}_0 | d_0)$, with $d_0 = \|\mathbf{p}_R\|_2$, i.e., the distribution of the gain depends only on the Tx-Rx distance. Thus, the integration over the radial component d_0 and the angular component $\theta_{T,0}$ of \mathbf{p}_R can be carried out separately. Then, as shown in the Appendix, we can reformulate (44) as an SDP using a one-dimensional (1D) quadrature rule for the approximation of the expectation integral over $\theta_{T,0}$.

For the power allocation vector \mathbf{q}_l , we consider only the l -th NLOS path and set the Rx position and orientation equal to the mean values $\bar{\mathbf{p}}_R$ and $\bar{\alpha}_R$ of their respective marginal prior distributions. This is basically a bistatic radar setup, where the goal is the estimation of the point of incidence. Therefore, we obtain \mathbf{q}_l by solving

$$\begin{aligned} \mathbf{q}_l &= \text{argmin}_{\mathbf{q}} \mathbb{E}_{\mathbf{p}_{s,l}} [\text{tr}(\mathbf{E}^T (\mathbb{E}_{|h_l| | \mathbf{p}_{s,l}} [\mathbf{J}_{\text{NLOS},l}(\mathbf{q}, \mathbf{p}_{s,l}, |h_l|)])^{-1} \mathbf{E})] \\ \text{s.t. } \mathbf{q} &\succeq \mathbf{0}, \quad \mathbf{1}^T \mathbf{q} \leq 1, \end{aligned} \quad (45)$$

where $\mathbf{J}_{\text{NLOS},l}$ represent the FIM for the parameter vector $\nu_{\text{NLOS},l} = [\mathbf{p}_{s,l}^T, \epsilon_{\text{clk}}, \mathbf{h}_l^T]^T$. Problem (45) can be solved employing a 2D cubature for the integration over $\mathbf{p}_{s,l}$.

Finally, we compute the optimal weights $\mathbf{w} \in \mathbb{R}^L$ of \mathbf{q}_l , $l = 0, \dots, L-1$, by minimizing an approximate lower bound on the ESPEB, obtained similarly to (43):

$$\begin{aligned} \mathbf{w} &= \text{argmin}_{\mathbf{w}} \mathbb{E}_{\mathbf{p}_R} [\text{tr}(\mathbf{E}^T \mathbf{J}^{-1}(\mathbf{Q} \mathbf{w}', \bar{\nu}) \mathbf{E})] \\ \text{s.t. } \mathbf{A}_0 \mathbf{Q} \mathbf{w}' &\succeq q_{\text{th}} \|\mathbf{A} \mathbf{Q} \mathbf{w}'\|_{\infty} \mathbf{1}_{N_{\theta}} \\ \mathbf{Q} \mathbf{w}' &\succeq \mathbf{0}, \quad \mathbf{1}^T \mathbf{Q} \mathbf{w}' \leq 1, \end{aligned} \quad (46)$$

where, in order to further reduce the computational load, we have replaced $\mathbb{E}_{\nu | \mathbf{p}_R}[\mathbf{J}(\mathbf{Q} \mathbf{w}', \nu)]$ with its approximation $\mathbf{J}(\mathbf{Q} \mathbf{w}', \bar{\nu})$, with $\bar{\nu} = \mathbb{E}_{\nu | \mathbf{p}_R}[\nu]$ and $\mathbf{Q} = [\mathbf{q}_0, \dots, \mathbf{q}_{L-1}]$. Finally, the beam power allocation vector is $\mathbf{q} = \mathbf{Q} \mathbf{w}$ and is referred to in the following as the suboptimal solution (subopt.). The computational complexity of this approach is dominated by the solution of (45) and (46), where 2D cubatures with a minimum of $2^{(r-1)/2}$ points can be employed.

V. CHANNEL AND POSITION ESTIMATION

In this section we present a novel two-stage algorithm for Rx position, orientation and clock offset estimation. In the first step, an off-grid parameter estimation approach, based on [43], is employed to recover the number paths and their respective TOAs, AODs and AOAAs. In the second step, the recovered channel parameters are mapped to the position parameter vector ν .

A. Channel Parameter Estimation

For our positioning purposes, we are not merely interested in denoising \mathbf{Y} , but we would like to recover the number of paths, along with their respective gains, TOAs, AODs and AOA. Hence, we aim to solve the following optimization problem:

$$\min_{L', \{\tau_l, \theta_{T,l}, \theta_{R,l}, h_l\}_{l=0}^{L'-1}} \Lambda(\mathbf{R}) + \chi \|\mathbf{h}\|_1, \quad (47)$$

where

$$\Lambda(\mathbf{R}) = \frac{1}{2} \|\mathbf{R}\|_F^2 \quad (48)$$

is the loss function,

$$\mathbf{R} = \mathbf{Y} - \sum_{l=0}^{L'-1} h_l \mathbf{C}(\tau_l, \theta_{T,l}, \theta_{R,l}) \quad (49)$$

is the residual, χ is a regularization parameter and $\mathbf{h} = [h_0, \dots, h_{L'-1}]^T$. The penalty term $\|\mathbf{h}\|_1$ is included to make the channel representation more parsimonious; otherwise the number of detected paths could grow arbitrarily so as to minimize the objective. As usual in sparse recovery setups, instead of a non-convex L0 norm penalty term, we use the L1 norm. We solve problem (47) using the algorithmic framework of [43], termed as Alternating Descent Conditional Gradient Method (ADCGM), which is described in Alg. 1. We note that, for notational brevity, in (47)-(49) and in the following, we write \mathbf{R} instead of $\mathbf{R}(L', \{\tau_l, \theta_{T,l}, \theta_{R,l}\}_{l=0}^{L'-1})$. Also, the residual at iteration i is denoted as \mathbf{R}_i and the TOAs of the detected paths are stacked in the vector $\boldsymbol{\tau}^{(i)} = [\tau_0^{(i)}, \dots, \tau_{L^{(i)}-1}^{(i)}] \in \mathbb{R}^{L^{(i)}}$, where $L^{(i)}$ is the number of detected paths at iteration i . The parameter vectors $\boldsymbol{\theta}_T^{(i)}$ and $\boldsymbol{\theta}_R^{(i)}$ are defined accordingly. The maximum number of iterations is L_{\max} and at each iteration a new path can be detected (Step 2) or previously detected paths can be dropped (Step 4(b)). In the following, we describe steps 2 and 4 in detail.

1) *Detection of a New Potential Path (Step 2)*: In order to get the next potential path we have to solve (50), which is non-convex and can be solved by discretizing the 3D parameter space $[0, T_{\text{CP}}] \times [-\pi, \pi] \times [-\pi, \pi]$ to get an $N_{\tau} \times N_{\theta_T} \times N_{\theta_R}$ -dimensional grid \mathcal{G} .

After computing the new potential source, we compare the corresponding objective with a predefined threshold $\zeta_1 > 0$, which is a function of the noise variance σ_{η}^2 , the reference signal \mathbf{X} and the desired false alarm probability P_{fa} .

2) *Coordinate Descent (Step 4)*: In this algorithmic step we iteratively perform 3 sub-steps for a fixed number of N_{cd} iterations:

- 1) We update the gains solving (51), keeping the other path parameters fixed. The regularization parameter χ determines the accuracy-sparsity trade-off.
- 2) We prune the paths whose gain is effectively zero: the l -th path is pruned if $|h_l|^2 / \zeta_2 < \max_{l=0, \dots, L^{(i)}-1} |h_l|^2$, where $0 < \zeta_2 \ll 1$.
- 3) For the local descent step we perform truncated Newton steps for each path and each parameter sequentially. The delay of the l -th path is updated as

$$\tau_l^{(i+1)} \leftarrow \tau_l^{(i+1)} - \text{sgn}(\partial \Lambda / \partial \tau_l^{(i+1)}) s_{\tau, l}^{(i+1)}, \quad (52)$$

Algorithm 1 Channel Parameter Estimation With ADCGM

input: $\{\mathbf{X}_b\}_{b=1}^{N_B}$, \mathbf{Y} , σ_{η}^2 , P_{fa}
initialize: $\boldsymbol{\tau}^{(0)}$, $\boldsymbol{\theta}_T^{(0)}$, $\boldsymbol{\theta}_R^{(0)}$, $\mathbf{h}^{(0)} = [\]$, $i = 0$
do

1. Compute residual \mathbf{R}_i
2. Detect next potential path:

$$\boldsymbol{\tau}^{(i)}, \boldsymbol{\theta}_T^{(i)}, \boldsymbol{\theta}_R^{(i)} = \underset{(\tau, \theta_T, \theta_R) \in \mathcal{G}}{\text{argmax}} \left| \text{tr}(\mathbf{R}_i^H \mathbf{C}(\tau, \theta_T, \theta_R)) \right| \quad (50)$$

3. Update support: $\boldsymbol{\tau}^{(i+1)} = [(\boldsymbol{\tau}^{(i)})^T, \boldsymbol{\tau}^{(i)}]^T$, $\boldsymbol{\theta}_T^{(i+1)} = [(\boldsymbol{\theta}_T^{(i)})^T, \boldsymbol{\theta}_T^{(i)}]^T$, $\boldsymbol{\theta}_R^{(i+1)} = [(\boldsymbol{\theta}_R^{(i)})^T, \boldsymbol{\theta}_R^{(i)}]^T$
4. Coordinate descent on non-convex objective:

for $j = 1$ to N_{cd} **do**

(a) Compute gains:

$$\mathbf{h}^{(i+1)} = \underset{\mathbf{h}}{\text{argmin}} \Lambda(\mathbf{R}) + \chi \|\mathbf{h}\|_1 \quad (51)$$

(b) Prune support:

$$\{\boldsymbol{\tau}, \boldsymbol{\theta}_T, \boldsymbol{\theta}_R, \mathbf{h}\}^{(i+1)} = \text{prune}(\{\boldsymbol{\tau}, \boldsymbol{\theta}_T, \boldsymbol{\theta}_R, \mathbf{h}\}^{(i+1)})$$

(c) Locally improve support:

$$\{\boldsymbol{\tau}, \boldsymbol{\theta}_T, \boldsymbol{\theta}_R\}^{(i+1)} = \text{local_descent}(\{\boldsymbol{\tau}, \boldsymbol{\theta}_T, \boldsymbol{\theta}_R, \mathbf{h}\}^{(i+1)})$$

end for

$i = i + 1$

while $i < L_{\max}$ and $|\text{tr}(\mathbf{R}_i^H \mathbf{C}(\boldsymbol{\tau}^{(i)}, \boldsymbol{\theta}_T^{(i)}, \boldsymbol{\theta}_R^{(i)}))| > \zeta_1$

where

$$s_{\tau, l}^{(i+1)} = \min \left(\left| \left(\frac{\partial^2 \Lambda}{(\partial \tau_l^{(i+1)})^2} \right)^{-1} \frac{\partial \Lambda}{\partial \tau_l^{(i+1)}} \right|, \frac{N_{\text{CP}} T_s}{2(N_{\tau} - 1)} \right)$$

is the step size, with $T_s = N \Delta f$. The AODs and AOAs are updated in a similar fashion. We note that we limit the maximum step size for each of the parameters to be equal to half of the corresponding grid bin size, in order to avoid convergence problems near inflection points of the loss function.

B. Mapping to Position Parameters

Having an estimate $\hat{\boldsymbol{\nu}}$ of the channel parameter vector $\boldsymbol{\nu}$ defined as

$$\hat{\boldsymbol{\nu}} = [\tau_0, \theta_{T,0}, \theta_{R,0}, \dots, \tau_{\hat{L}-1}, \theta_{T,\hat{L}-1}, \theta_{R,\hat{L}-1}]^T, \quad (53)$$

where \hat{L} is the estimated number of paths, and choosing the strongest path as the LOS path, we estimate the position parameter vector $\boldsymbol{\nu}$ employing the EXIP as in [13], with a slight modification to include the prior information on the clock offset. To this end, we intend to solve

$$\underset{\boldsymbol{\nu}}{\text{argmin}} (\hat{\boldsymbol{\nu}} - f(\boldsymbol{\nu}))^T \mathbf{J}_{\hat{\boldsymbol{\nu}}} (\hat{\boldsymbol{\nu}} - f(\boldsymbol{\nu})) + (\epsilon_{\text{clk}} / \sigma_{\text{clk}})^2, \quad (54)$$

where $\mathbf{J}_{\hat{\boldsymbol{\nu}}}$ is the channel parameter FIM and $f : \mathbb{R}^{2\hat{L}+2} \rightarrow \mathbb{R}^{3\hat{L}}$ is the mapping from position to channel parameters, determined by (4), (7)-(8).

We note that false alarms, that is falsely detected paths, can have severe impact on position estimation. Therefore, we apply the following two criteria to filter them out:

- A single-bounce NLOS path and a LOS path always form a triangle, as can be seen in Fig. 1. Such formation of a triangle is possible if a single-bounce NLOS path satisfies

$$\Delta\theta_{T,l} \cdot \Delta\theta_{R,l} < 0, \quad l = 1, \dots, \hat{L} - 1, \quad (55)$$

where $\Delta\theta_{T,l} = \theta_{T,l} - \theta_{T,0}$ and $\Delta\theta_{R,l} = \theta_{R,l} - \theta_{R,0}$, with $\Delta\theta_{T,l}$ and $\Delta\theta_{R,l} \in [-\pi, \pi)$. Therefore if the l -th path, $l = 1, \dots, \hat{L} - 1$, does not satisfy (55), it is dropped.

- Combined with the LOS path, each NLOS path forms a triangle, which provides a system of 3 equations with 3 unknowns $d_{l,1} = \|\mathbf{p}_{s,l}\|_2$, $d_{l,2} = \|\mathbf{p}_R - \mathbf{p}_{s,l}\|_2$ and ϵ_{clk} :

$$d_{l,1} + d_{l,2} = c(\tau_l - \epsilon_{\text{clk}}), \quad (56a)$$

$$d_{l,1} \sin(\Delta\theta_{T,l}) = -d_{l,2} \sin(\Delta\theta_{R,l}), \quad (56b)$$

$$d_{l,1} \cos(\Delta\theta_{T,l}) + d_{l,2} \cos(\Delta\theta_{R,l}) = c(\tau_0 - \epsilon_{\text{clk}}). \quad (56c)$$

By solving (56a) for each path separately we get an estimate of ϵ_{clk} :

$$\begin{aligned} & \hat{\epsilon}_{\text{clk},l} \\ &= \frac{\tau_l \sin(\Delta\theta_{R,l} - \Delta\theta_{T,l}) - \tau_0 (\sin(\Delta\theta_{R,l}) - \sin(\Delta\theta_{T,l}))}{\sin(\Delta\theta_{R,l} - \Delta\theta_{T,l}) - (\sin(\Delta\theta_{R,l}) - \sin(\Delta\theta_{T,l}))}. \end{aligned} \quad (57)$$

With $\zeta_{3,a} > 0$ and $\zeta_{3,b} > 0$ being predefined probability thresholds for estimated ϵ_{clk} values, if $p_{\epsilon_{\text{clk}}}(\hat{\epsilon}_{\text{clk},l}) < \zeta_{3,a}$ or $p_{\epsilon_{\text{clk}}}(\hat{\epsilon}_{\text{clk},l}) < \zeta_{3,b} p_{\text{clk,max}}$, the path is filtered out, with $p_{\text{clk,max}} = \max_{l=1, \dots, \hat{L}-1} p(\hat{\epsilon}_{\text{clk},l})$. The intuition behind both these conditions is the following: Due to their randomness, the parameters of falsely detected paths, which correspond to noise, will generally result in very unlikely values of clock offset estimates from (57) and can consequently be rejected by the first condition. The reason for including the second condition, is that combined with a low $\zeta_{3,a}$ value, it allows us to prevent rejection of existing paths, while still rejecting false alarms, in the case of less likely ϵ_{clk} realizations.

Replacing $\hat{\mathbf{v}}$ with $\hat{\mathbf{v}}'$, which contains only the remaining paths, we solve (54) with the Levenberg-Marquardt algorithm [55], [56]. For the initial point $\boldsymbol{\nu}^{(0)}$ we compute

$$\epsilon_{\text{clk}}^{(0)} = \frac{\sum_l |h_l|^2 \hat{\epsilon}_{\text{clk},l}}{\sum_l |h_l|^2}, \quad (58)$$

$$\mathbf{p}_R^{(0)} = c(\tau_0 - \epsilon_{\text{clk}}^{(0)}) \mathbf{u}(\theta_{T,0}), \quad (59)$$

$$\alpha_R^{(0)} = \theta_{T,0} + \pi - \theta_{R,0}, \quad (60)$$

and

$$\mathbf{p}_{s,l}^{(0)} = \frac{\tan(\theta_{R,l} + \alpha_R^{(0)}) p_{R,x}^{(0)} - p_{R,y}^{(0)}}{\tan(\theta_{R,l} + \alpha_R^{(0)}) \cos \theta_{T,l} - \sin \theta_{T,l}} \mathbf{u}(\theta_{T,l}), \quad (61)$$

for $l = 1, \dots, \hat{L}'$, where \hat{L}' is the number of remaining estimated paths.

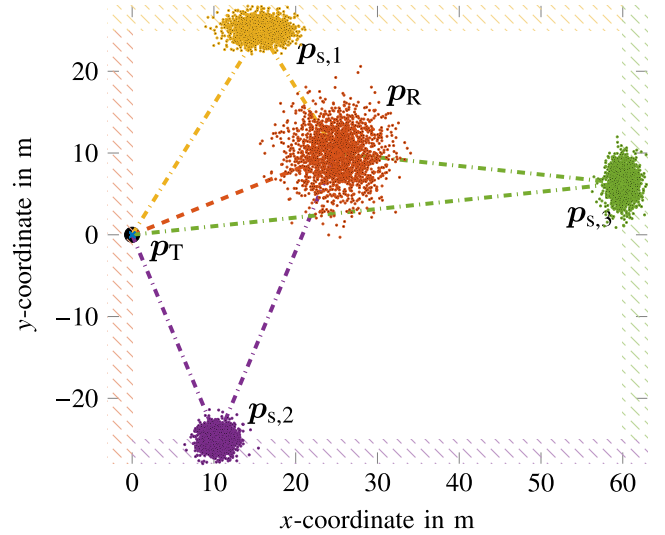


Fig. 2. Prior knowledge at the Tx for simulation results.

VI. NUMERICAL RESULTS

A. Simulation Setup

For the evaluation of the power allocation and the position estimation algorithms we consider the setup shown in Fig. 2. The Tx is equipped with a uniform linear array (ULA) with $N_T = 32$ antennas. In order to be able to discriminate all possible AOAs, the Rx has a uniform circular array (UCA) with $N_R = 16$ antennas. With the Rx being equipped with a UCA, the SPEB is independent of the orientation α_R .

We consider NLOS paths resulting from single-bounce reflections. The phases of the complex path gains are uniformly distributed over $[-\pi, \pi)$ and their magnitudes are given by

$$|h_l| = \begin{cases} c/(4\pi f_c \|\mathbf{p}_R\|_2), & l = 0, \\ \sqrt{\rho_l} c / (4\pi f_c (\|\mathbf{p}_{s,l}\|_2 + \|\mathbf{p}_R - \mathbf{p}_{s,l}\|_2)), & l \neq 0, \end{cases} \quad (62)$$

where ρ_l is the reflection coefficient and $\lambda_c = c/f_c$. The prior knowledge at the Tx is described by $\mathcal{N}(\boldsymbol{\mu}, \mathbf{C})$, where

$$\begin{aligned} \boldsymbol{\mu} &= [\bar{\mathbf{p}}_R^T, \bar{\mathbf{p}}_{s,1}^T, \bar{\rho}, \bar{\mathbf{p}}_{s,2}^T, \bar{\rho}, \bar{\mathbf{p}}_{s,3}^T, \bar{\rho}]^T \in \mathbb{R}^{11}, \quad (63) \\ \mathbf{C} &= \begin{bmatrix} \mathbf{C}_{0,0} & \mathbf{C}_{0,1} & \mathbf{0} & \mathbf{C}_{0,2} & \mathbf{0} & \mathbf{C}_{0,3} & \mathbf{0} \\ \mathbf{C}_{0,1}^T & \mathbf{C}_{1,1} & \mathbf{0} & \mathbf{0} & \mathbf{0} & \mathbf{0} & \mathbf{0} \\ \mathbf{0} & \mathbf{0} & \sigma_\rho^2 & \mathbf{0} & \mathbf{0} & \mathbf{0} & \mathbf{0} \\ \mathbf{C}_{0,2}^T & \mathbf{0} & \mathbf{0} & \mathbf{C}_{2,2} & \mathbf{0} & \mathbf{0} & \mathbf{0} \\ \mathbf{0} & \mathbf{0} & \mathbf{0} & \mathbf{0} & \sigma_\rho^2 & \mathbf{0} & \mathbf{0} \\ \mathbf{C}_{0,3}^T & \mathbf{0} & \mathbf{0} & \mathbf{0} & \mathbf{0} & \mathbf{C}_{3,3} & \mathbf{0} \\ \mathbf{0} & \mathbf{0} & \mathbf{0} & \mathbf{0} & \mathbf{0} & \mathbf{0} & \sigma_\rho^2 \end{bmatrix} \in \mathbb{R}^{11 \times 11}, \quad (64) \end{aligned}$$

with

$$\begin{aligned} \bar{\mathbf{p}}_R &= \begin{bmatrix} 25 \\ 10 \end{bmatrix} \text{ m}, \quad \mathbf{C}_{0,0} = 4/\sqrt{2} \mathbf{I}_2 \text{ m}^2, \\ \bar{\mathbf{p}}_{s,1} &= \begin{bmatrix} 15.63 \\ 25 \end{bmatrix} \text{ m}, \quad \mathbf{C}_{1,1} = \begin{bmatrix} 3.48 & 0 \\ 0 & 1 \end{bmatrix} \text{ m}^2, \quad \mathbf{C}_{0,1} = \begin{bmatrix} 4.45 & 0 \\ 0 & 0 \end{bmatrix} \text{ m}^2, \\ \bar{\mathbf{p}}_{s,2} &= \begin{bmatrix} 10.42 \\ -25 \end{bmatrix} \text{ m}, \quad \mathbf{C}_{2,2} = \begin{bmatrix} 1.34 & 0 \\ 0 & 1 \end{bmatrix} \text{ m}^2, \quad \mathbf{C}_{0,2} = \begin{bmatrix} 1.64 & 0 \\ 0 & 0 \end{bmatrix} \text{ m}^2, \end{aligned}$$

$$\bar{\mathbf{p}}_{s,3} = \begin{bmatrix} 60 \\ 6.32 \end{bmatrix} \text{ m}, \quad \mathbf{C}_{3,3} = \begin{bmatrix} 1 & 0 \\ 0 & 2.31 \end{bmatrix} \text{ m}^2, \quad \mathbf{C}_{0,3} = \begin{bmatrix} 0 & 0 \\ 0 & 3.24 \end{bmatrix} \text{ m}^2, \\ \bar{\rho} = -10 \text{ dB}, \quad \sigma_\rho = 4 \text{ dB}.$$

Samples from this distribution are depicted in Fig. 2.

For the waveform we set $f_c = 38 \text{ GHz}$, $N = 64$, $N_B = 10$, $\mathcal{P} = \{-31, \dots, -1, 1, \dots, 31\}$ and $\Delta f(\max(\mathcal{P}) - \min(\mathcal{P}))(\approx B) = 120 \text{ MHz}$. The resources are assigned to the beams in an interleaved and staggered manner, i.e., $\mathcal{R}_k = \{(k + b + iM_T, b) | i \in \mathbb{Z}, b = 1, \dots, N_B : k + b + iM_T \in \mathcal{P}\}$. The power of each beam is distributed uniformly among its resources, i.e., $\gamma_k[p, b] = 1/|\mathcal{R}_k|$. The noise variance is $\sigma_\eta^2 = 10^{0.1(n_{\text{Rx}} + N_0)} N \Delta f$, where $N_0 = -174 \text{ dBm Hz}^{-1}$ is the noise power spectral density per dimension and $n_{\text{Rx}} = 8 \text{ dB}$ is the Rx noise figure. The standard deviation of the clock offset is equal to the 2 sample intervals, i.e., $\sigma_{\text{clk}} = 2/(N \Delta f)$, so that $c\sigma_{\text{clk}} \approx 4.88 \text{ m}$. We use a DFT beam codebook:

$$\mathbf{f}_k = [1, e^{-j\frac{2\pi}{N_T}k}, \dots, e^{-j\frac{2\pi}{N_T}(N_T-1)k}], \quad k = 1, \dots, M_T = N_T. \quad (65)$$

Regarding the position estimation algorithm parameters, we set $N_\tau = 2 N_P$, $N_{\theta_T} = 2 N_T$, $N_{\theta_R} = 2 N_R$, $P_{\text{fa}} = 0.05$, ζ_1 is pre-trained for the given P_{fa} and power allocation strategy, $\zeta_2 = -35 \text{ dB}$, $N_{\text{cd}} = 3$, $L_{\text{max}} = 10$, $\chi = \sigma_\eta \sqrt{2(N_T + N_R)} |P| N_B P_{\text{RE}} / N_T$ (chosen according to [57]), $\zeta_{3,a} = 10^{-4}$ and $\zeta_{3,b} = 10^{-2}$.

B. Power Allocation Strategies

We consider the power allocation strategies discussed in Sec. IV. To fairly evaluate our power allocation strategies, we set as a benchmark the uniform power allocation to beams exciting useful directions. We refer to this strategy as “uni” in the following. The corresponding details of each approach are as follows:

- *opt. unconstr.*: The number of points of known cubatures of 5th degree (in order to ensure a sufficiently dense sampling of the support of the distribution) with positive weights is $2^{11} + 2 \cdot 11 = 2070$ [53], which incurs prohibitive computational complexity. To make it manageable, we instead draw $11^2 = 121$ random samples (as many as the lower bound for any cubature) from the joint 11-dimensional distribution.
- *opt. constr.*: We draw 121 random samples from the joint 11-dimensional distribution and set $\kappa = 0.995$, $q_{\text{th}} = -10 \text{ dB}$ and $N_\theta = 15$.
- *opt. reduced*: We draw $8^2 = 64$ random samples from the joint 8-dimensional distribution and set $\kappa = 0.995$, $q_{\text{th}} = -10 \text{ dB}$ and $N_\theta = 15$.
- *subopt.*: We use 9-point cubatures for the involved 2D marginals and set $\kappa = 0.995$, $q_{\text{th,LOS}} = -3 \text{ dB}$, $q_{\text{th}} = -10 \text{ dB}$ and $N_\theta = 15$.
- *uni*: For a given confidence level κ we get a grid of AODs for each path as in (39) and compute the set of useful beams as

$$\mathcal{B}_{\text{uni}}^{(\kappa)} = \bigcup_{l=0}^{L-1} \bigcup_{m=0}^{N_\theta} \left\{ \text{argmax}_{k=1, \dots, N_T} |\mathbf{a}_T^T(\theta_{T,l,m}^{(\kappa)}) \mathbf{f}_k| \right\}. \quad (66)$$

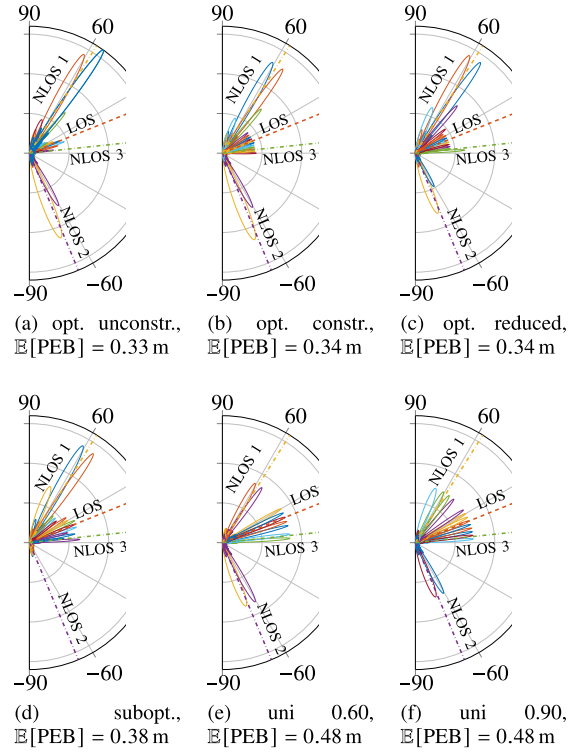


Fig. 3. Beam patterns $|\mathbf{a}_T^T(\theta_T) \mathbf{f}_k \sqrt{q_k}|$, $k = 1, \dots, M_T$, for different power allocation strategies.

The power allocation vector \mathbf{q} is

$$q_k = \begin{cases} 1/|\mathcal{B}_{\text{uni}}^{(\kappa)}|, & k \in \mathcal{B}_{\text{uni}}^{(\kappa)}, \\ 0, & k \notin \mathcal{B}_{\text{uni}}^{(\kappa)}. \end{cases} \quad (67)$$

We set again $N_\theta = 15$. We consider two values for κ , namely $\kappa = 0.60$ and $\kappa = 0.9$, and refer to the resulting power allocation strategies as “uni 0.60” and “uni 0.90”. We note that choosing $\kappa = 0.995$ as for the other strategies results in performance degradation; hence, results for this value are not included.

The beampatterns of the power allocation strategies for the considered prior knowledge are shown in Fig. 3. We also show the sample average PEB, which is denoted as $\mathbb{E}[\text{PEB}]$ and computed by drawing 2000 random samples from the prior. We observe in Figs. 3(a)-(d) that for the optimized power allocation strategies, most of the available power is used on beams illuminating NLOS paths. The reason for this is that for non-perfect Tx-Rx synchronization (i.e., $\sigma_{\text{clk}} = 2/(N \Delta f)$), neither the LOS nor a NLOS path provide individually sufficient information about the Tx-Rx distance, because the TOA measurements cannot be reliably translated to distances. Only when σ_{clk} is very small (i.e., when the synchronization error is very small), having only the delay measurement of the LOS suffices to determine the distance between the BS and the UE. However, when the synchronization error is not small, it is the differences between delays that are informative, and this implies that several paths (not only one) have to be illuminated with sufficient power.

Furthermore, when comparing Fig. 3(a) with Figs. 3(b)-(d), we see that when the constraints (41) are not applied, the power allocation to NLOS components is higher, with the power invested to less likely LOS directions being very low. From Figs. 3(b) and (c), we can see that the impact of the dimensionality reduction (43) is the reduction of the power used on the 2nd NLOS path. This is explained by the fact that the fading of the path gains is not taken into account; hence, for the mean values of the path gains, more power is used on the paths that offer more useful position information. Also, in Fig. 3(d) we observe that our suboptimal approach allocates almost no power to the 2nd NLOS path, as in the last step, where all paths are considered jointly, only the receiver's location uncertainty and the mean locations of scatterers/reflectors are taken into account. For this setup, the information offered by the 1st NLOS path is more useful and therefore most of the available power is allocated for its illumination. For the uniform allocation, higher confidence values lead to activation of more beams and spreading of the available power to more directions.

Regarding the achievable positioning accuracy of the different power allocation strategies, we see that "opt. unconstr." achieves the lowest $\mathbb{E}[\text{PEB}]$, with "opt. constr." and "opt. reduced" having almost the same performance. The reduced complexity for the computation of the "subopt." power allocation incurs a slight performance penalty, but the resulting $\mathbb{E}[\text{PEB}]$ is still significantly lower than that of the uniform power allocation strategies.

C. Positioning Accuracy for Fixed Geometry

We fix the geometry and the reflection coefficients to their mean value μ in (63) to examine the position estimation accuracy as a function of the Tx power. For the power allocation strategies described in Sec. VI-B, in Fig. 4, we plot the position root mean square error (RMSE) $\sqrt{\mathbb{E}_{\eta, \epsilon_{\text{clk}}}[\|\hat{\mathbf{p}}_{\text{R}} - \mathbf{p}_{\text{R}}\|_2^2]}$ and PEB as functions of the average power per resource element $P_{\text{RE}} = P_{\text{tot}}/(N_{\text{B}}N_{\text{P}})$, with $\hat{\mathbf{p}}_{\text{R}}$ being the position estimate. We note that the average Tx power P_{T} is related to P_{RE} as $P_{\text{T}} = P_{\text{RE}}N_{\text{P}}/N$.

Similar to our conclusions in Sec. VI-B, we observe that the PEB attained with the "opt. unconstr." power allocation is slightly lower than those of "opt. constr.", "opt. reduced" and "subopt.", which are approximately equal. The PEBs of the above-mentioned power allocations are significantly lower than those of the benchmarking uniform power allocations.

We now examine the performance of the power allocation strategies using the position estimation algorithm, i.e., we compare them with respect to their RMSE. Regarding the performance of the position estimation algorithm itself, due to space limitations, a detailed comparison with [13] was not possible, but we have verified that the proposed method leads to improved performance with respect to [13]. We can see in Fig. 4 that the bound is attained for all power allocation strategies, with the P_{RE} value for which the RMSE converges to the PEB being different for each strategy. Regarding uniform power allocation, the gap of the RMSE to the bound for low Tx power is attributed to the fact that, although the

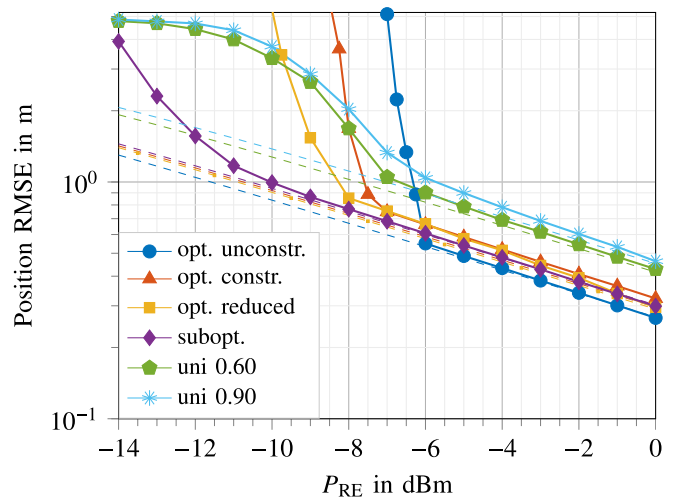


Fig. 4. Position RMSE (solid lines) and PEB (dashed lines) vs Tx power for different power allocation strategies.

LOS path is detected, the probability of detection for the NLOS is small. With only the LOS path being detected, the clock offset cannot be resolved and the resulting position RMSE approaches the standard deviation of the clock offset $c \cdot \sigma_{\text{clk}} \approx 4.88$ m. Among the two considered configurations ($\kappa = 0.60$ and $\kappa = 0.90$), the former has slightly better performance, as the available power is more concentrated to the true location of the Rx and the reflectors. However, this comes at a cost, when the uncertainty about the geometry is considered (as discussed in Sec. VI-D).

The optimized allocation strategies ("opt. unconstr.", "opt. constr.", "opt. reduced" and "subopt.") result in similar PEBs and offer significant improvement compared to the uniform ones, with a gain of 3 to 4 dB for the same localization accuracy. The lowest PEB is attained by "opt. unconstr.", but the RMSE converges to the PEB for larger P_{RE} , compared to the other strategies. The reason for this behavior is that, as can be observed in Fig. 3(a), only a small fraction of power is used in the LOS direction and the Tx power required for the LOS path to be detected is larger. When the LOS path is missed, the first arriving NLOS path is treated as LOS by the algorithm, resulting in a large position error. Due to the constraints (41), the rest of the proposed strategies ("opt. constr.", "opt. reduced" and "subopt.") allocate more power to the LOS, enabling the algorithm to attain the PEB at lower values of P_{RE} , with only a small performance penalty. The RMSE of "opt. reduced" converges slightly faster to the bound compared to "opt. constr.", as slightly more power is allocated to the LOS path. The "subopt." allocation exhibits the most robust performance, as the LOS path can be detected for much lower Tx power values.

D. Positioning Accuracy With Random Samples

The results in Fig. 4 and the corresponding discussion in Sec. VI-C are useful in comparing the power allocation strategies and evaluating the convergence of the position estimation algorithm for a varying signal-to-noise ratio (SNR), but do

TABLE I
PERCENTILES OF THE CDF OF THE POSITION ERROR IN m FOR
DIFFERENT POWER ALLOCATION STRATEGIES

	50%	90%	95%	99%
opt. unconstr.	0.22	0.93	29.55	72.25
opt. constr.	0.21	0.59	0.78	1.32
opt. reduced	0.21	0.57	0.76	1.25
subopt.	0.21	0.65	0.84	1.45
uni 0.60	0.31	0.91	1.30	20.83
uni 0.90	0.30	0.86	1.10	1.96

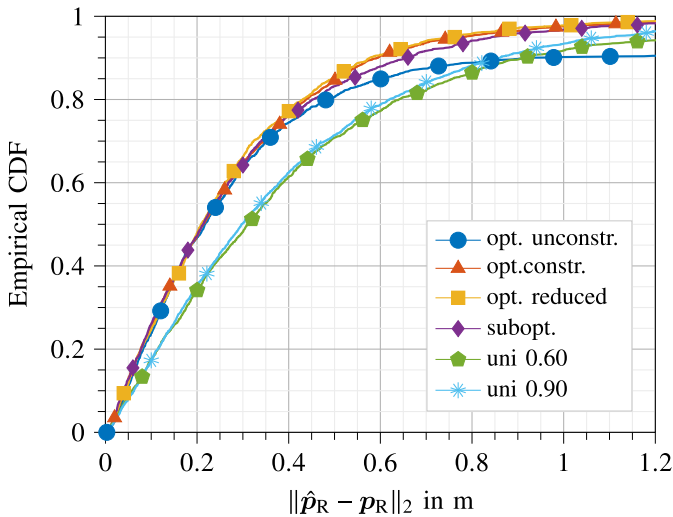


Fig. 5. Empirical cdf of $\|\hat{\mathbf{p}}_R - \mathbf{p}_R\|_2$ for different power allocation strategies.

not provide a complete characterization of the performance of the power allocation strategies. To better examine their performance, for $P_{RE} = 0$ dBm and the rest of the system parameters as described in Sec. VI-A, we plot in Fig. 5 the cumulative distribution function (cdf) of the position error $\|\hat{\mathbf{p}}_R - \mathbf{p}_R\|_2$, which is computed by drawing samples from (63)-(64). A summary of the percentiles of the distribution of the position error is provided in Table I.

We can observe in Fig. 5 and Table I that “opt. reduced” and “opt. constr.” achieve the best performance. The latter is slightly worse at higher percentiles, as more points would be required for a more accurate approximation of the expectation in the corresponding optimization problem. In spite of the lower computational cost of the “subopt.” allocation, its performance degradation is almost unnoticeable. On the other hand, the “opt. unconstr.” approach, although attaining almost the same median error as the other optimized strategies, has much lower accuracy for higher percentiles. This is attributed to the low power used in the direction around the LOS path, resulting in low probability of detection of the LOS. Compared to the best of the uniform allocations, the “opt. reduced” power allocation offers a position error reduction of 30%, 34%, 31% and 36% at the 50%, 90%, 95% and 99% percentile, respectively.

Regarding the uniform allocations, we can see that spreading the power to a reduced set of beams (“uni 0.60”) might result in better positioning accuracy for some geometry

realizations, as seen for example in Fig. 4, but it significantly deteriorates the performance for other possible realizations. This explains the higher values of position errors at the upper percentiles of the corresponding cdf.

E. Impact of Synchronization Quality

We now examine the effect of synchronization quality, as captured by σ_{clk} , on the power allocation and the positioning accuracy. First, similar to (66), we define the set of LOS-illuminating beams as

$$\mathcal{B}_{\text{LOS}}^{(\kappa)} = \cup_{m=0}^{N_\theta} \left\{ \text{argmax}_{k=1, \dots, N_T} |\mathbf{a}_T^T(\theta_{T,0,m}^{(\kappa)}) \mathbf{f}_k| \right\} \quad (68)$$

and the fraction of power used on them as

$$q_{\text{LOS}} = \sum_{k \in \mathcal{B}_{\text{LOS}}^{(\kappa)}} q_k. \quad (69)$$

In Fig. 6(a) we plot q_{LOS} as a function of σ_{clk} for the power allocation strategies “opt. unconstr.,” “opt. constr.,” “subopt” and “uni 0.90”, for $N_R = \{4, 16\}$, $P_{RE} = 0$ dBm, $\kappa = 0.995$ and the rest of the system parameters as described in Sec. VI-A; in Fig. 6(b) we plot the corresponding $\mathbb{E}[\text{PEB}]$. We can see in Fig. 6(a) that for very low values of σ_{clk} , equivalent to almost perfect Tx-Rx synchronization, it is optimal to use almost all the available power on LOS-illuminating beams. As σ_{clk} increases, q_{LOS} decreases rapidly for all optimized allocation strategies, until it saturates at a relatively low value. This is explained as follows: The clock offset decreases the amount of distance information provided by the LOS path; the larger the standard deviation of the clock offset, the more significant the decrease. This can be understood from (4) and (14), where we can see that the values ϵ_{clk} determine how reliably the LOS delay measurement can be translated to distance measurement. As σ_{clk} increases, ϵ_{clk} is likely to take values which are significantly different from zero, making the distance measurement from the LOS path unreliable. Hence, as σ_{clk} increases, the distance information provided by the NLOS paths becomes more significant and, therefore, more power is used on them. Nevertheless, the saturation occurs because the measurement of the LOS AOD offers significant information in the orthogonal direction, which is reduced when q_{LOS} is decreased. The saturation value for “opt. constr.” is higher due to the additional constraints on LOS illumination.

Furthermore, we observe that the transition from high to low q_{LOS} values is slower for $N_R = 4$. This is attributed to the fact that NLOS paths offer rank-1 position information, whose intensity depends on the quality of the TOA, AOD and AOA measurements combined [11], [12]. Therefore, the intensity of the information from the NLOS paths is smaller for $N_R = 4$ than for $N_R = 16$, as the quality of the AOA measurement is poorer. Consequently, for larger values of σ_{clk} , the information from the NLOS paths becomes significant relative to the LOS distance information.

In Fig. 6(b) it can be observed that $\mathbb{E}[\text{PEB}]$ increases with increasing σ_{clk} , until it saturates at a value dependent on the power allocation strategy and the system configuration ($N_R = \{4, 16\}$). As σ_{clk} increases the reduction of distance information from the LOS path cannot be complemented by distance information from the NLOS paths (even with

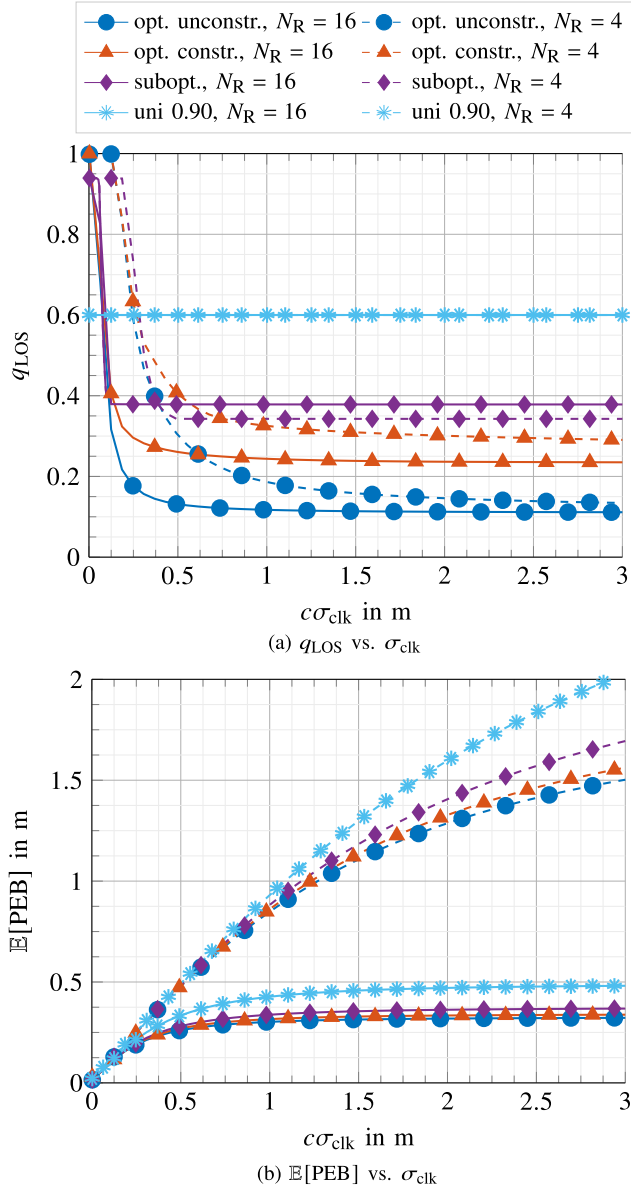


Fig. 6. Fraction of power allocated to LOS-illuminating beams q_{LOS} and $\mathbb{E}[\text{PEB}]$ as functions of $c\sigma_{\text{clk}}$.

optimized power allocation), resulting in a larger error. In the saturation region the distance information from the LOS path becomes negligible compared to the clock offset-independent part of distance information offered by the combination of NLOS paths with the LOS path.

VII. CONCLUSION

Optimal power allocation for single-anchor localization using a beam codebook and lower-complexity suboptimal alternatives have been considered under imperfect Tx-Rx synchronization. A channel and position estimation method has also been proposed. Numerical results show that our suboptimal power allocation approach offers a good balance between performance and complexity, as the significant reduction of the power-allocation complexity incurs only a very small performance degradation. While these results have been

observed in general and not only for the considered setup, more simulations would be appropriate to exactly quantify the performance variation in a broader set of cases. Our analysis has shown that, even for small clock offset standard deviation, it is optimal in the CRLB sense to allocate most of the available power to scatterer/reflector illuminating beams to recover necessary range information. We have also shown that guaranteeing a minimum amount of power used on LOS-illuminating beams, can be beneficial when the actual position estimation is considered, as it ensures that the LOS path is detected with a high probability. The proposed position estimation algorithm reaches the corresponding CRLB for all considered power allocation strategies. It avoids the appearance of spurious paths due to grid mismatch, by benefiting from the off-grid estimation of channel parameters. In addition, noisy detected paths are filtered out exploiting the information on the clock offset carried by single-bounce-NLOS paths.

APPENDIX

POWER ALLOCATION FOR THE LOS PATH

Here we show how to formulate (44) as an SDP using only a 1D quadrature rule for the approximation of the expectation over $\theta_{T,0}$. This is accomplished in two steps:

- In the first step we show that the integration over d_0 and $\theta_{T,0}$ can be carried out separately;
- in the second step, after averaging over d_0 , we exploit the form of the resulting function of $\theta_{T,0}$ and formulate the problem as an SDP.

We write $\mathbb{E}_{d_0, \theta_{T,0}}[\cdot]$ instead of $\mathbb{E}_{\mathcal{P}_R}[\cdot]$. Also, for notational brevity we write

$$\bar{\mathbf{J}} = \mathbb{E}_{\alpha_R, \mathbf{h}_0 | d_0, \theta_{T,0}} [\mathbf{J}_{\nu_{\text{LOS}}}(\mathbf{q}, d_0, \theta_{T,0}, \alpha_R, \mathbf{h}_0)]. \quad (70)$$

We index the elements of $\bar{\mathbf{J}}$ with the pair of parameters to which they correspond.

First, after some algebra we find that

$$\begin{aligned} \text{tr}(\mathbf{E}^T \bar{\mathbf{J}}^{-1} \mathbf{E}) &= \frac{c^2}{\bar{J}_{\tau_0, \tau_0} - \frac{\bar{J}_{\tau_0, \theta_{T,0}}^2}{\bar{J}_{\theta_{T,0}, \theta_{T,0}}}} \\ &+ \frac{d_0^2}{\bar{J}_{\theta_{T,0}, \theta_{T,0}} - \frac{\bar{J}_{\tau_0, \theta_{T,0}}^2}{\bar{J}_{\tau_0, \tau_0}}} + c^2 \sigma_{\text{clk}}^2, \end{aligned} \quad (71)$$

where

$$\bar{J}_{a,b} = \mathbb{E}_{\alpha_R, \mathbf{h}_0 | d_0, \theta_{T,0}} [J_{a,b}], \quad (72)$$

$$J_{a,b} = \frac{2}{\sigma_\eta^2} \sum_{b=1}^{N_B} \sum_{p \in \mathcal{P}} \Re \left\{ \frac{\partial \mathbf{m}_b^H[p]}{\partial a} \frac{\partial \mathbf{m}_b[p]}{\partial b} \right\}, \quad (73)$$

with $a, b \in \{d_0, \theta_{T,0}\}$. We can show that $J_{a,b}$, $a, b \in \{d_0, \theta_{T,0}\}$, are independent of α_R and the phase of \mathbf{h}_0 . Hence, they can be expressed as

$$\begin{aligned} \bar{J}_{a,b} &= \mathbb{E}_{\mathbf{h}_0 | d_0, \theta_{T,0}} [J_{a,b}(\mathbf{q}, \theta_{T,0}, |h_0(d_0)|^2)] \\ &= \mathbb{E}_{\mathbf{h}_0 | d_0, \theta_{T,0}} [|h_0(d_0)|^2 j_{a,b}(\mathbf{q}, \theta_{T,0})] \\ &= g_0(d_0) j_{a,b}(\mathbf{q}, \theta_{T,0}), \end{aligned} \quad (74)$$

where $g_0(d_0) = \mathbb{E}_{\mathbf{h}_0 | d_0} [|h_0(d_0)|^2]$ and $j_{a,b}(\mathbf{q}, \theta_{T,0}) = J_{a,b}(\mathbf{q}, \theta_{T,0}, |h_0(d_0)|^2) / |h_0(d_0)|^2$ is a function of \mathbf{q} and $\theta_{T,0}$.

For the second equality in (74), we used the fact that $J_{a,b}$ can be expressed as the product of two terms, one dependent on the gain magnitude and the other on \mathbf{q} and $\theta_{T,0}$. We can then rewrite (71) as

$$\text{tr}(\mathbf{E}^T \bar{\mathbf{J}}^{-1} \mathbf{E}) = \frac{1}{g_0(d_0)} \left(\frac{c^2}{I_{\tau_0}(\mathbf{q}, \theta_{T,0})} + \frac{d_0^2}{I_{\theta_{T,0}}(\mathbf{q}, \theta_{T,0})} \right) + c^2 \sigma_{\text{clk}}^2, \quad (75)$$

where

$$I_{\tau_0}(\mathbf{q}, \theta_{T,0}) = j_{\tau_0, \tau_0}(\mathbf{q}, \theta_{T,0}) - \frac{j_{\tau_0, \theta_{T,0}}^2(\mathbf{q}, \theta_{T,0})}{j_{\theta_{T,0}, \theta_{T,0}}(\mathbf{q}, \theta_{T,0})}, \quad (76)$$

$$I_{\theta_{T,0}}(\mathbf{q}, \theta_{T,0}) = j_{\theta_{T,0}, \theta_{T,0}}(\mathbf{q}, \theta_{T,0}) - \frac{j_{\tau_0, \theta_{T,0}}^2(\mathbf{q}, \theta_{T,0})}{j_{\tau_0, \tau_0}(\mathbf{q}, \theta_{T,0})}. \quad (77)$$

It is apparent from (75) that integration of the function over d_0 and $\theta_{T,0}$ can be carried out separately.

For the second step, taking the expectation over d_0 and defining

$$\bar{g}_0(\theta_{T,0}) = 1/\mathbb{E}_{d_0|\theta_{T,0}}[1/g_0(d_0)] \quad (78)$$

$$\bar{d}_0(\theta_{T,0}) = \sqrt{\mathbb{E}_{d_0|\theta_{T,0}} \left[\frac{\bar{g}_0(\theta_{T,0})}{g_0(d_0)} d_0^2 \right]} \quad (79)$$

we get

$$\mathbb{E}_{d_0|\theta_{T,0}}[\text{tr}(\mathbf{E}^T \bar{\mathbf{J}}^{-1} \mathbf{E})] = \frac{1}{\bar{g}_0(\theta_{T,0})} \left(\frac{c^2}{I_{\tau_0}(\mathbf{q}, \theta_{T,0})} + \frac{(\bar{d}_0(\theta_{T,0}))^2}{I_{\theta_{T,0}}(\mathbf{q}, \theta_{T,0})} \right) + c^2 \sigma_{\text{clk}}^2. \quad (80)$$

Comparing (80) to (71), we can conclude that, in order to be able to formulate the problem in a convex form, $\mathbb{E}_{d_0|\theta_{T,0}}[\text{tr}(\mathbf{E}^T \bar{\mathbf{J}}^{-1} \mathbf{E})]$ can be expressed as

$$\mathbb{E}_{d_0|\theta_{T,0}}[\text{tr}(\mathbf{E}^T \bar{\mathbf{J}}^{-1} \mathbf{E})] = \text{tr}(\mathbf{E}^T \mathbf{J}_{\nu_{\text{LOS}}}^{-1}(\mathbf{q}, \bar{d}_0(\theta_{T,0}), \theta_{T,0}, \check{\alpha}_R, \sqrt{\bar{g}_0(\theta_{T,0})} e^{j\beta_g}) \mathbf{E}), \quad (81)$$

where $\check{\alpha}_R$ and β_g can be chosen arbitrarily, since they do not have an impact on the objective. Finally, using (81) and the identity

$$\mathbb{E}_{d_0, \theta_{T,0}}[\text{tr}(\mathbf{E}^T \bar{\mathbf{J}} \mathbf{E})] = \mathbb{E}_{\theta_{T,0}}[\mathbb{E}_{d_0|\theta_{T,0}}[\text{tr}(\mathbf{E}^T \bar{\mathbf{J}}^{-1} \mathbf{E})]], \quad (82)$$

we can employ a 1D quadrature rule to approximate the expectation integral over $\theta_{T,0}$ to get the following SDP:

$$\begin{aligned} & \min_{\mathbf{q}, \mathbf{B}_1, \dots, \mathbf{B}_{N_{\theta_{T,0}}}} \sum_{j=1}^{N_{\theta_{T,0}}} p_j \text{tr}(\mathbf{B}_j) \\ & \text{s.t. } \mathbf{q} \geq \mathbf{0}, \mathbf{1}^T \mathbf{q} \leq 1, \\ & \begin{bmatrix} \mathbf{B}_j & \mathbf{E}^T \\ \mathbf{E} \mathbf{J}_{\nu_{\text{LOS}}}(\mathbf{q}, \bar{d}_0(\theta_{T,0,j}), \theta_{T,0,j}, \check{\alpha}_R, \sqrt{\bar{g}_0(\theta_{T,0,j})} e^{j\beta_g}) \end{bmatrix} \succeq \mathbf{0}, \\ & j = 1, \dots, N_{\theta_{T,0}}. \end{aligned} \quad (83) \end{aligned}$$

REFERENCES

- [1] S. Mumtaz, J. Rodriguez, and L. Dai, *mmWave Massive MIMO: A Paradigm for 5G*. New York, NY, USA: Academic, 2017.
- [2] A. L. Swindlehurst, E. Ayanoglu, P. Heydari, and F. Capolino, "Millimeter-wave massive MIMO: The next wireless revolution?" *IEEE Commun. Mag.*, vol. 52, no. 9, pp. 56–62, Sep. 2014.
- [3] F. Wen, H. Wymeersch, B. Peng, W. P. Tay, H. C. So, and D. Yang, "A survey on 5G massive MIMO localization," *Digit. Signal Process.*, vol. 94, pp. 21–28, Nov. 2019.
- [4] R. Keating, M. Saily, J. Hultkonen, and J. Karjalainen, "Overview of positioning in 5G new radio," in *Proc. 16th Int. Symp. Wireless Commun. Syst. (ISWCS)*, Aug. 2019, pp. 320–324.
- [5] J. A. del Peral-Rosado, R. Raulefs, J. A. Lopez-Salcedo, and G. Seco-Granados, "Survey of cellular mobile radio localization methods: From 1G to 5G," *IEEE Commun. Surveys Tuts.*, vol. 20, no. 2, pp. 1124–1148, 2nd Quart., 2018.
- [6] 3rd Generation Partnership Project (3GPP), *Technical Specification Group Services and System Aspects; Study on Positioning Use Cases; Stage 1 (Release 16)*, document TR22.872 V16.1.0, Aug. 2019.
- [7] H. Wymeersch, G. Seco-Granados, G. Destino, D. Dardari, and F. Tufvesson, "5G mmWave positioning for vehicular networks," *IEEE Wireless Commun.*, vol. 24, no. 6, pp. 80–86, Dec. 2017.
- [8] A. Shahmansoori, G. E. Garcia, G. Destino, G. Seco-Granados, and H. Wymeersch, "5G position and orientation estimation through millimeter wave MIMO," in *Proc. IEEE Globecom Workshops (GC Wkshps)*, San Diego, CA, USA, Dec. 2015, pp. 1–6.
- [9] Z. Abu-Shaban, X. Zhou, T. D. Abhayapala, G. Seco-Granados, and H. Wymeersch, "Error bounds for uplink and downlink 3D localization in 5G millimeter wave systems," *IEEE Trans. Wireless Commun.*, vol. 17, no. 8, pp. 4939–4954, Aug. 2018.
- [10] A. Guerra, F. Guidi, and D. Dardari, "Single-anchor localization and orientation performance limits using massive arrays: MIMO vs. Beamforming," *IEEE Trans. Wireless Commun.*, vol. 17, no. 8, pp. 5241–5255, Aug. 2018.
- [11] R. Mendrzik, H. Wymeersch, G. Bauch, and Z. Abu-Shaban, "Harnessing NLOS components for position and orientation estimation in 5G millimeter wave MIMO," *IEEE Trans. Wireless Commun.*, vol. 18, no. 1, pp. 93–107, Jan. 2019.
- [12] A. Kakkavas, M. H. Castaneda Garcia, R. A. Stirling-Gallacher, and J. A. Nossek, "Performance limits of single-anchor millimeter-wave positioning," *IEEE Trans. Wireless Commun.*, vol. 18, no. 11, pp. 5196–5210, Nov. 2019.
- [13] A. Shahmansoori, G. E. Garcia, G. Destino, G. Seco-Granados, and H. Wymeersch, "Position and orientation estimation through millimeter-wave MIMO in 5G systems," *IEEE Trans. Wireless Commun.*, vol. 17, no. 3, pp. 1822–1835, Mar. 2018.
- [14] J. Talvitie, M. Koivisto, T. Levanen, M. Valkama, G. Destino, and H. Wymeersch, "High-accuracy joint position and orientation estimation in sparse 5G mmWave channel," in *Proc. IEEE Int. Conf. Commun. (ICC)*, Shanghai, China, May 2019, pp. 1–7.
- [15] J. Palacios, G. Bielsa, P. Casari, and J. Widmer, "Single- and multiple-access point indoor localization for millimeter-wave networks," *IEEE Trans. Wireless Commun.*, vol. 18, no. 3, pp. 1927–1942, Mar. 2019.
- [16] Y. Liu, Y. Shen, and M. Z. Win, "Single-anchor localization and synchronization of full-duplex agents," *IEEE Trans. Commun.*, vol. 67, no. 3, pp. 2355–2367, Mar. 2019.
- [17] T. Wang, H. Zhao, and Y. Shen, "An efficient single-anchor localization method using ultra-wide bandwidth systems," *Appl. Sci.*, vol. 10, no. 1, p. 57, Dec. 2019.
- [18] M. Rath, J. Kulmer, E. Leitinger, and K. Witrals, "Single-anchor positioning: Multipath processing with non-coherent directional measurements," *IEEE Access*, vol. 8, pp. 88115–88132, May 2020.
- [19] A. Fascista, A. Coluccia, H. Wymeersch, and G. Seco-Granados, "Millimeter-wave downlink positioning with a single-antenna receiver," *IEEE Trans. Wireless Commun.*, vol. 18, no. 9, pp. 4479–4490, Sep. 2019.
- [20] A. Fascista, A. Coluccia, H. Wymeersch, and G. Seco-Granados, "Low-complexity accurate mmwave positioning for single-antenna users based on angle-of-departure and adaptive beamforming," in *Proc. IEEE Int. Conf. Acoust., Speech Signal Process. (ICASSP)*, Barcelona, Spain, May 2020, pp. 4866–4870.
- [21] C. Gentner, T. Jost, W. Wang, S. Zhang, A. Dammann, and U.-C. Fiebig, "Multipath assisted positioning with simultaneous localization and mapping," *IEEE Trans. Wireless Commun.*, vol. 15, no. 9, pp. 6104–6117, Sep. 2016.

- [22] E. Leitinger, F. Meyer, F. Hlawatsch, K. Witrals, F. Tufvesson, and M. Z. Win, "A belief propagation algorithm for multipath-based SLAM," *IEEE Trans. Wireless Commun.*, vol. 18, no. 12, pp. 5613–5629, Dec. 2019.
- [23] H. Wymeersch *et al.*, "5G mmWave downlink vehicular positioning," in *Proc. IEEE Global Commun. Conf. (GLOBECOM)*, Abu Dhabi, UAE, Dec. 2018, pp. 206–212.
- [24] J. Talvitie, T. Levanen, M. Koivisto, K. Pajukoski, M. Renfors, and M. Valkama, "Positioning of high-speed trains using 5G new radio synchronization signals," in *Proc. IEEE Wireless Commun. Netw. Conf. (WCNC)*, Apr. 2018, pp. 1–6.
- [25] X. Li, E. Leitinger, M. Oskarsson, K. Astrom, and F. Tufvesson, "Massive MIMO-based localization and mapping exploiting phase information of multipath components," *IEEE Trans. Wireless Commun.*, vol. 18, no. 9, pp. 4254–4267, Sep. 2019.
- [26] R. Mendrzik, F. Meyer, G. Bauch, and M. Z. Win, "Enabling situational awareness in millimeter wave massive MIMO systems," *IEEE J. Sel. Topics Signal Process.*, vol. 13, no. 5, pp. 1196–1211, Sep. 2019.
- [27] H. Kim, K. Granstrom, S. Kim, and H. Wymeersch, "Low-complexity 5g SLAM with CKF-PHD filter," in *Proc. IEEE Int. Conf. Acoust., Speech Signal Process. (ICASSP)*, Barcelona, Spain, May 2020, pp. 5220–5224.
- [28] B. Zhou, A. Liu, and V. Lau, "Successive localization and beamforming in 5G mmWave MIMO communication systems," *IEEE Trans. Signal Process.*, vol. 67, no. 6, pp. 1620–1635, Mar. 2019.
- [29] N. Garcia, H. Wymeersch, and D. T. M. Slock, "Optimal precoders for tracking the AoD and AoA of a mmWave path," *IEEE Trans. Signal Process.*, vol. 66, no. 21, pp. 5718–5729, Nov. 2018.
- [30] R. Koirala, B. Denis, D. Dardari, and B. Uguen, "Localization bound based beamforming optimization for multicarrier mmWave MIMO," in *Proc. 14th Workshop Positioning, Navigat. Commun. (WPNC)*, Bremen, Germany, Oct. 2017, pp. 1–6.
- [31] R. Koirala, B. Denis, B. Uguen, D. Dardari, and H. Wymeersch, "Localization optimal multi-user beamforming with multi-carrier mmWave MIMO," in *Proc. IEEE 29th Annu. Int. Symp. Pers., Indoor Mobile Radio Commun. (PIMRC)*, Bologna, Italy, Sep. 2018, pp. 1–7.
- [32] H. Zhao, L. Zhang, and Y. Shen, "On the optimal beamspace design for direct localization systems," in *Proc. IEEE Int. Conf. Commun. (ICC)*, Kansas City, MO, USA, May 2018, pp. 1–6.
- [33] H. Zhao, N. Zhang, and Y. Shen, "Robust beamspace design for direct localization," in *Proc. IEEE Int. Conf. Acoust., Speech Signal Process. (ICASSP)*, Brighton, U.K., May 2019, pp. 4360–4364.
- [34] W. W.-L. Li, Y. Shen, Y. J. Zhang, and M. Z. Win, "Robust power allocation for energy-efficient location-aware networks," *IEEE/ACM Trans. Netw.*, vol. 21, no. 6, pp. 1918–1930, Dec. 2013.
- [35] A. Shahmansoori, G. Seco-Granados, and H. Wymeersch, "Power allocation for OFDM wireless network localization under expectation and robustness constraints," *IEEE Trans. Wireless Commun.*, vol. 16, no. 3, pp. 2027–2038, Mar. 2017.
- [36] Y. Shen, W. Dai, and M. Z. Win, "Power optimization for network localization," *IEEE/ACM Trans. Netw.*, vol. 22, no. 4, pp. 1337–1350, Aug. 2014.
- [37] M. F. Keskin, A. D. Sezer, and S. Gezici, "Localization via visible light systems," *Proc. IEEE*, vol. 106, no. 6, pp. 1063–1088, Jun. 2018.
- [38] A. Kakkavas, G. Seco-Granados, H. Wymeersch, M. H. C. Garcia, R. A. Stirling-Gallacher, and J. A. Nossek, "5G downlink multi-beam signal design for LOS positioning," in *Proc. IEEE Global Commun. Conf. (GLOBECOM)*, Waikoloa, HI, USA, Dec. 2019, pp. 1–6.
- [39] R. Vaughan and J. Bach-Anderson, *Channels, Propagation and Antennas for Mobile Communications* (Electromagnetic Waves). Stevenage, U.K.: The Institution of Engineering and Technology, 2003.
- [40] T. S. Rappaport, E. Ben-Dor, J. N. Murdock, and Y. Qiao, "38 GHz and 60 GHz angle-dependent propagation for cellular & peer-to-peer wireless communications," in *Proc. IEEE Int. Conf. Commun. (ICC)*, Ottawa, ON, Canada, Jun. 2012, pp. 4568–4573.
- [41] M.-T. Martinez-Ingles, D. P. Gaillot, J. Pascual-Garcia, J.-M. Molina-Garcia-Pardo, M. Lienard, and J.-V. Rodriguez, "Deterministic and experimental indoor mmW channel modeling," *IEEE Antennas Wireless Propag. Lett.*, vol. 13, pp. 1047–1050, 2014.
- [42] M. Peter *et al.* (Mar. 2016). *Measurement Campaigns and Initial Channel Models for Preferred Suitable Frequency Ranges; Deliverable D2.1*. [Online]. Available: <https://5g-mmmagic.eu/results/#deliverables>
- [43] N. Boyd, G. Schiebinger, and B. Recht, "The alternating descent conditional gradient method for sparse inverse problems," *SIAM J. Optim.*, vol. 27, no. 2, pp. 616–639, Jan. 2017.
- [44] T. E. Abrudan, A. Haghparast, and V. Koivunen, "Time synchronization and ranging in OFDM systems using time-reversal," *IEEE Trans. Instrum. Meas.*, vol. 62, no. 12, pp. 3276–3290, Dec. 2013.
- [45] K.-L. Noh, Q. M. Chaudhari, E. Serpedin, and B. W. Suter, "Novel clock phase offset and skew estimation using two-way timing message exchanges for wireless sensor networks," *IEEE Trans. Commun.*, vol. 55, no. 4, pp. 766–777, Apr. 2007.
- [46] H. Godrich, A. M. Haimovich, and H. V. Poor, "An analysis of phase synchronization mismatch sensitivity for coherent MIMO radar systems," in *Proc. 3rd IEEE Int. Workshop Comput. Adv. Multi-Sensor Adapt. Process. (CAMSAP)*, Dec. 2009, pp. 153–156.
- [47] J. Elson, L. Girod, and D. Estrin, "Fine-grained network time synchronization using reference broadcasts," *ACM SIGOPS Operating Syst. Rev.*, vol. 36, pp. 147–163, Dec. 2002.
- [48] A. Dammann, T. Jost, R. Raulefs, M. Walter, and S. Zhang, "Optimizing waveforms for positioning in 5G," in *Proc. IEEE 17th Int. Workshop Signal Process. Adv. Wireless Commun. (SPAWC)*, Edinburgh, U.K., Jul. 2016, pp. 1–5.
- [49] M. D. Larsen, G. Seco-Granados, and A. L. Swindlehurst, "Pilot optimization for time-delay and channel estimation in OFDM systems," in *Proc. IEEE Int. Conf. Acoust., Speech Signal Process. (ICASSP)*, Prague, Czech Republic, May 2011, pp. 3564–3567.
- [50] A. Shahmansoori, G. Seco-Granados, and H. Wymeersch, "Robust power allocation for OFDM wireless network localization," in *Proc. IEEE Int. Conf. Commun. Workshop (ICCW)*, London, U.K., Jun. 2015, pp. 718–723.
- [51] Y. Rockah and P. Schultheiss, "Array shape calibration using sources in unknown locations—Part I: Far-field sources," *IEEE Trans. Acoust., Speech, Signal Process.*, vol. 35, no. 3, pp. 286–299, Mar. 1987.
- [52] H. Messer, "The hybrid Cramer-Rao lower bound—From practice to theory," in *Proc. 4th IEEE Workshop Sensor Array Multichannel Process.*, Waltham, MA, USA, Jul. 2006, pp. 304–307.
- [53] R. Cools, "An encyclopaedia of cubature formulas," *J. Complex.*, vol. 19, no. 3, pp. 445–453, Jun. 2003.
- [54] D. Crouse, "Basic tracking using nonlinear 3D monostatic and bistatic measurements," *IEEE Aerosp. Electron. Syst. Mag.*, vol. 29, no. 8, pp. 4–53, Aug. 2014.
- [55] K. Levenberg, "A method for the solution of certain non-linear problems in least squares," *Quart. Appl. Math.*, vol. 2, no. 2, pp. 164–168, Jul. 1944.
- [56] D. W. Marquardt, "An algorithm for least-squares estimation of nonlinear parameters," *J. Soc. Ind. Appl. Math.*, vol. 11, no. 2, pp. 431–441, Jun. 1963.
- [57] P. Zhang, L. Gan, S. Sun, and C. Ling, "Atomic norm denoising-based channel estimation for massive multiuser MIMO systems," in *Proc. IEEE Int. Conf. Commun. (ICC)*, London, U.K., Jun. 2015, pp. 4564–4569.



His research interests include mm-Wave communications, positioning, and probabilistic inference.



His current research interests include the convergence of communication and sensing, in a 5G and beyond 5G context. He served as an Associate Editor for IEEE COMMUNICATION LETTERS from 2009 to 2013, IEEE TRANSACTIONS ON WIRELESS COMMUNICATIONS since 2013, and IEEE TRANSACTIONS ON COMMUNICATIONS from 2016 to 2018. From 2019 to 2021, he was the IEEE Distinguished Lecturer with the Vehicular Technology Society.

Anastasios Kakkavas (Graduate Student Member, IEEE) received the Diploma degree in electrical and computer engineering from the National Technical University of Athens (NTUA), Athens, Greece, in 2012, and the M.Sc. degree in communications engineering from the Technical University of Munich (TUM), Munich, Germany, in 2015, where he is currently pursuing the Ph.D. degree with the Department of Electrical and Computer Engineering. He joined the Munich Research Center, Huawei Technologies Duesseldorf GmbH, Munich, in 2015.

Henk Wymeersch (Senior Member, IEEE) received the Ph.D. degree in electrical engineering/applied sciences from Ghent University, Belgium, in 2005. From 2005 to 2009, he was a Post-Doctoral Researcher with the Laboratory for Information and Decision Systems, Massachusetts Institute of Technology. He is currently a Professor of communication systems with the Department of Electrical Engineering, Chalmers University of Technology, Sweden. He is also a Distinguished Research Associate with the Eindhoven University of Technology.



Gonzalo Seco-Granados (Senior Member, IEEE) received the Ph.D. degree in telecommunications engineering from the Universitat Politècnica de Catalunya, Spain, in 2000, and the M.B.A. degree from the IESE Business School, Spain, in 2002. From 2002 to 2005, he was a member of the European Space Agency, where he was involved in the design of the Galileo system and receivers. He was a Fulbright Visiting Scholar with the University of California at Irvine, Irvine, CA, USA, in 2015 and 2019. From 2011 to 2019, he has worked as the Vice Dean of the Engineering School, Universitat Autònoma de Barcelona. He is currently a Professor with the Department of Telecommunication, Universitat Autònoma de Barcelona. His research interests include statistical signal processing with application to GNSS and 5G localization. Since 2018, he has been serving as a member of the Sensor Array and Multichannel Technical Committee for the IEEE Signal Processing Society. Since 2019, he has been the President of the Spanish Chapter of the IEEE Aerospace and Electronic Systems Society.



Mario H. Castañeda García (Member, IEEE) received the B.Sc. degree in electrical engineering from the Universidad Nacional Autónoma de Honduras, Tegucigalpa, Honduras, in 2001, and the M.Sc. degree in communications engineering and the Dr.-Ing. degree from the Technische Universität München (TUM), Munich, Germany, in 2004 and 2014, respectively. From 2005 to 2014, he was a Research and a Teaching Assistant with the Institute for Circuit Theory and Signal Processing, TUM, where he was involved in several industry and government projects in the areas of signal processing for wireless communication systems and for satellite-based positioning. He joined the Munich Research Center, Huawei Technologies Düsseldorf GmbH, Munich, in 2014, where he has been involved in several EU funded research projects as well as in 5G research and standardization activities. His research interests include multi-antenna technologies, millimeter-wave systems, V2X communication, and wireless positioning. He was the recipient of the Best Overall Paper Award at IEEE VTC Fall 2018.



Richard A. Stirling-Gallacher (Member, IEEE) received the M.Eng. degree in electronic engineering from the University of Southampton, U.K., in 1990, and the Ph.D. degree from The University of Edinburgh, U.K., in 1997. From 1997 to 2012, he was a Principal Researcher with Sony Deutschland GmbH, Stuttgart, Germany, where he led wireless system and algorithmic research for 3G, 4G, and millimeter-wave (mm-wave)-based communication systems. From 2012 to 2014, he was with Samsung Research America, Dallas, TX, USA, where he led research and pre-standardization for mm-wave and massive multi in multi out (MIMO) for 5G New Radio. He joined Huawei Technologies Inc., San Diego, CA, USA, in 2014, and subsequently in 2017, transferred to the Munich Research Center, Huawei Technologies Duesseldorf GmbH, Munich, Germany, as a Research Expert/Team Leader. He currently holds more than 110 granted U.S. patents. His current research interests include integrated communications and sensing, positioning, massive MIMO, and V2X for beyond 5G communication systems.



Josef A. Nossek (Life Fellow, IEEE) received the Dipl.-Ing. and Dr. Techn. degrees in electrical engineering from the Vienna University of Technology, Austria, in 1974 and 1980, respectively. He joined Siemens AG, Munich, Germany, as a Member of Technical Staff, in 1974, where he became a Supervisor in 1978, and was the Head of the Department in 1980. He was promoted to be Head of all radio systems design in 1987. Since 1989, he has been a Full Professor of circuit theory and signal processing with the Munich University of Technology, where he teaches undergraduate and graduate courses on circuit and systems theory and signal processing and leads research on signal processing algorithms for communications, especially multi-antenna systems. From 2016 to 2019, he was a Full Professor with the Federal University of Ceará, Brazil. His awards include the ITG Best Paper Award 1988, the Mannesmann Mobilfunk (now Vodafone) Innovations Award 1998, and the Award for Excellence in Teaching from the Bavarian Ministry for Science, Research and Art in 1998. He received the Golden Jubilee Medal for Outstanding Contributions to the Society and the Education Award from the IEEE Circuits and Systems Society in 1999 and 2008, respectively. He also received the Order of Merit of the Federal Republic of Germany in 2008. He was an Elected Member of the German National Academy of Engineering Sciences (acatech) in 2009. He received an Honorary Doctorate in 2013 and the Ring of Honor from VDE in 2014. He was the Elected President, the President, and the Past President of the IEEE Circuits and Systems Society in 2001, 2002, and 2003, respectively. From 2005 to 2010, he was the Vice President of VDE (Verband der Elektrotechnik, Elektronik und Informationstechnik e.V.).